Open Research Online

The Open University's repository of research publications
and other research outputs

A photoionization-modelling study of 30 Doradus: the case for small-scale chemical inhomogeneity

Journal Item

oro.open.ac.uk

A photoionization-modelling study of 30 Doradus: the case for small-scale chemical inhomogeneity

Yiannis G. Tsamis⋆†‡ and Daniel Péquignot
LUTH, Laboratoire l'Univers et ses Théories, associé au CNRS (FRE 2462) et á l'Université Paris 7, Observatoire de Paris-Meudon, F-92195 Meudon Cédex, France

ABSTRACT

Photoionization models of the giant H II region (GHIIR) 30 Doradus are built and confronted to available ultraviolet (UV), optical, infrared (IR) [*Infrared Space Observatory* (*ISO*)] and radio spectra, under blackbody or *CoStar* spectral energy distributions for the primary source and various density distributions for the nebular gas. Chemically homogeneous models show very small rms electron-temperature fluctuations and fail to reproduce the heavy-element optical recombination line (ORL) spectrum of the nebula. Dual-abundance models incorporating small-scale chemical inhomogeneities in the form of hydrogen-deficient inclusions which are in pressure balance with the normal-composition ambient gas, provide a better fit to the observed heavy-element ORLs *and* other nebular lines, while most spectral features are satisfactorily accounted for. The inclusions, whose mass is ∼2 per cent of the total gaseous mass, are 2–3 times cooler and denser than the ambient nebula. Their O/H abundance ratio is ∼0.9 dex larger than in the normal-composition gas and have typical mass fractions of $X = 0.687$, $Y = 0.273$ and $Z = 0.040$. Helium is found to be about as deficient as hydrogen in the inclusions, while elements heavier than neon, such as sulphur and argon, are quite possibly enhanced in proportions similar to oxygen, as indicated by the most satisfactory dual-abundance model obtained. This suggests that the posited hydrogen-deficient inclusions may have arisen from partial mixing of matter which was nucleosynthetically processed in a supernova event with gas of normal Large Magellanic Cloud composition. The average gaseous abundances of the chemically inhomogeneous models are ∼0.08 dex higher than those of the homogeneous models, yet they are lower by a similar ∼0.08 dex than those derived from standard empirical methods (fully corrected for inaccuracies in ionization correction factors and differences in atomic data) which postulate temperature fluctuations in a chemically homogeneous medium. Attention is drawn to a bias in the determination of H II region (HIIR) helium abundances in the presence of hydrogen-deficient inclusions. It is argued that these results provide evidence for incomplete small-scale mixing of the interstellar medium (ISM). The case for the existence of abundance inhomogeneities in HIIRs is examined in the light of current theoretical considerations regarding the process of chemical homogenization in the ISM.

Key words: ISM: abundances – ISM: evolution – H II regions – ISM: individual: 30 Doradus – galaxies: individual: LMC.

1 INTRODUCTION

The emission-line analysis of ionized gaseous nebulae such as planetary nebulae (PNe; ionized ejected envelopes of low- to intermediate-mass evolved stars) and H II regions (HIIRs) (ionized gas clouds marking the birth places of stars, like the Orion Nebula) is one of the best established methods for obtaining the abundance of elements in our own and in external galaxies. Abundance studies of PNe reveal the composition of matter returned to the interstellar medium (ISM) after being processed by stellar nucleosynthesis, while those of HIIRs provide a snapshot of the composition of the ISM in the latest episode of its evolution.

Since before the 1990s, a source of controversy in the field has arisen from the fact that, for both PNe and HIIRs, the abundances

⋆E-mail: ygt@star.ucl.ac.uk
†Present address: Department of Physics and Astronomy, University College London, Gower Street, London WC1E 6BT.
‡P. Gruber Foundation/IAU Fellow.

of carbon, nitrogen, oxygen and neon (relative to hydrogen) based on optical recombination lines (ORLs) are found to be consistently higher than the abundances of the same elements derived from their ultraviolet (UV), optical and infrared (IR) collisionally excited lines (CELs; Barker 1984; Peimbert, Storey & Torres-Peimbert 1993; Rola & Stasińska 1994; Liu et al. 1995, 2000, 2001, 2004; Tsamis et al. 2003a,b, 2004; Esteban et al. 2005). The ORL/CEL ionic abundance discrepancy factors (ADFs) for O^{2+} and C^{2+} have been shown to be strongly correlated with the difference between the nebular electron temperatures derived from the nebular to auroral [O III] optical-line ratio and the H I Balmer recombination continuum break at 3646 Å (Liu et al. 2001; Tsamis 2002; Tsamis et al. 2004).

Deciphering the thermal and density structures of ionized nebulae is a very important matter in its own right, given the exponential dependence of CEL-based abundances on the adopted nebular electron temperature (T_e; e.g. Osterbrock 1989) and the possibility that such abundances might be largely in error, that is, underestimated, in the case of strong fluctuations in temperature (e.g. Peimbert 1967) or density (e.g. Rubin 1989) within the nebular volumes. *Hubble Space Telescope* (*HST*) observations of the optical [O III] nebular-to-auroral-line ratio in the Orion Nebula, where the ADF is small, revealed residual small-scale temperature fluctuations (O'Dell, Peimbert & Peimbert 2003), whose origin has not been fully elucidated. However, it has now become clear that invoking in all generality the presence of such fluctuations in a chemically homogeneous medium fails to account consistently for the observed behaviour of the ADFs; chiefly the fact that these do not correlate with the excitation energies or critical densities of the lines in question. This is true for PNe (Liu et al. 2000; Tsamis et al. 2003b, 2004) and for HIIRs (Tsamis et al. 2003a, hereafter T03). In parallel, the recent downward revision of the solar oxygen abundance (Allende Prieto & Lambert 2001) has removed the long-lasting impression that the oxygen abundances of Galactic PNe were lower than that of the Sun and possibly therefore only lower limits: mean PN oxygen abundances derived from forbidden lines (Kingsburgh & Barlow 1994; Exter, Barlow & Walton 2004) are now in good agreement with solar values. Finally, recent spectroscopic results making use of the weakly T_e-dependent ratios of O II ORLs have provided evidence for the presence of a very low-temperature ($\lesssim 10^3$ K) gaseous component embedded within both typical PNe (Tsamis et al. 2004) and atypical 'born-again' PNe (Wesson, Liu & Barlow 2003).

The question of whether the supersonic velocities and induced shocks from Wolf–Rayet stellar winds and supernova remnants (SNRs) (e.g. Chu & Kennicutt 1994) might produce significant temperature fluctuations within giant H II regions (GHIIRs), unaccounted for by static photoionization codes, warrants further analysis: however, as long as the ORL/CEL abundance discrepancies are found to be uncorrelated with the excitation energies of the various CELs, the answer to the above question does not bear heavily on the ORL/CEL abundance discrepancy issue.

The currently most viable explanation for both the ORL/CEL abundance dichotomy and the very low temperatures derived from recombination lines or continua, posits the existence within nebulae of a gas component enhanced in heavy elements and therefore efficiently cooled by emission in fine-structure CELs (Liu et al. 2000; Péquignot et al. 2002; Tsamis et al. 2004). This material which is traced by the emission of weak heavy-element ORLs, is intermingled with a more normal-composition, hotter ($\sim 10^4$ K) medium, traced by the emission of strong CELs. The above picture has gained in credibility since it has been supported by dual-abundance photoionization models of PNe (Péquignot et al. 2002, 2003; Ercolano

et al. 2003; Tylenda 2003; Tsamis & Péquignot 2004; Tsamis & Péquignot, in preparation).

From the standpoint of chemical-abundance analyses, an important result of the dual-abundance model is that the high-metallicity component comprises only a small fraction (~ 1 per cent) of the total ionized nebular mass in the objects considered so far, so that the heavy-element content of the nebulae is closer to the one given by the classical forbidden-line analysis (Péquignot et al. 2002; Tsamis et al. 2004). This contrasts with the classical temperature-fluctuation paradigm, which invariably leads to CNONe abundances closer to those given by the ORL method for PNe (Ruiz et al. 2003; Peimbert et al. 2004) and for HIIRs (Peimbert 2003, hereafter P03; Esteban et al. 2005, and references therein). Since emission-line studies of HIIRs provide a wealth of information regarding elemental abundances in extragalactic systems and therefore have a considerable bearing on cosmic chemical-evolution studies, the question of which description provides the right answer is a pressing one.

The co-existence, in PNe, of gas phases with very different compositions and temperatures may plausibly result from the ejection of material from the evolving central star whose surface composition changes as nuclear reactions and mass loss proceed, as in, for example, the 'born-again PN' scenario (Iben et al. 1983). This is perhaps more unexpected in HIIRs which are recently ionized zones of the 'normal' ISM. These objects, however, are not born *ex nihilo*. Their chemical composition depends on the past history of the host galaxy: the thorough mixing of the ISM is a long process in which successive generations of massive stars may be involved (e.g. Tenorio-Tagle 1996). They are also dynamic systems, hosting potential sources of chemical inhomogeneities, such as SNRs, evolved massive O/Wolf–Rayet (WR)-type stars subject to extensive mass loss via stellar winds, and photoevaporating protoplanetary discs.[1] In the face of recent studies which have uncovered fairly large ADFs (~ 2–5 for O^{2+}) for Galactic and extragalactic HIIRs (Esteban et al. 2002; T03), efforts should be directed at clarifying the situation.

In this paper, we present a photoionization model study of the 30 Doradus nebula for which high-quality, multiwaveband spectroscopy has become available in recent years, including the heavy-element ORLs of interest. We would like to investigate whether, by analogy with PNe, the existence of chemical inhomogeneities could provide a solution to the ORL/CEL problem for this class of nebulae as well, and thus help us choose between the two conflicting abundance sets. In Section 2, we collate available spectroscopic data pertinent to this study, while in Section 3 we present the models and results. Finally, in Section 4 we discuss the implications of this work for emission-line studies of photoionized nebulae and consider various hypotheses on the likely nature and origin of the postulated chemical inhomogeneities in HIIRs.

2 OBSERVATIONS

At an adopted distance of 50 kpc, the 30 Doradus nebula in the Large Magellanic Cloud (LMC) is the closest extragalactic GHIIR in our cosmic neighbourhood. Its full extent in Hα emission is well over a degree in diameter ($\simeq 1$ kpc). It is photoionized by a tremendous amount of Lyman-continuum (Ly-c) radiation whose total flux has

---

[1] 30 Doradus contains both SNRs (such as N157B; e.g. Lazendic, Dickel & Jones 2003) and numerous Wolf–Rayet stars (see Parker 1993; Crowther & Dessart 1998), while a plethora of 'proplyds' have been identified in, for example, the Orion Nebula.

been estimated to be up to $\sim 10^{52}$ photons s^{-1} from radio observations of the entire nebula (Mills, Turtle & Watkinson 1978), while almost half of this (4.2×10^{51} photons s^{-1}) arises from within the inner 10 pc, provided by 117 massive OB- and WR-type stars of the R136 cluster in the core of the nebula (Crowther & Dessart 1998). The integrated (reddened) Hα flux of the central 30 arcmin is 1.71×10^{-8} erg cm^{-2} s^{-1} (Kennicutt & Hodge 1986), corresponding to 4.2×10^{51} photons s^{-1} in the Ly continuum.

Over the years, the nebula has been observed extensively from UV to radio wavelengths. In this study, we made use of optical emission-line fluxes by P03 [Ultraviolet and Visual Echelle Spectrograph of the Very Large Telescope (UVES/VLT) 8.2 m] and T03 [ESO Multi-Mode Instrument of the New Technology Telescope (EMMI/NTT) 3.6 m]; UV fluxes by Dufour et al. (1982; *International Ultraviolet Explorer* [*IUE*] and Garnett et al. (1995a,b; *HST* Faint Object Spectrograph [FOS]); IR fluxes by Vermeij et al. (2002; *Infrared Space Observatory* [*ISO*] Short Wavelength Spectrometer [SWS] and Long Wavelength Spectrometer [LWS]), except for the [Ar II] 6.98-µm line noted by Giveon et al. (2002); and radio fluxes by Filipovic et al. (1995). A compilation of these is provided in Table 3 [column 3; de-reddened intensities expressed in units such that $I(\mathrm{H}\beta)=10^3$].

The *ISO* SWS and LWS data are for the position '30 Doradus #3' of Vermeij et al. (2002); the positions observed optically by T03 and P03 fell within this pointing and the 80-arcsec LWS circular beam. Peimbert's 3×10-arcsec^2 échelle slit was placed on a bright filamentary 'ridge' located 64 arcsec north and 60 arcsec east from HD 38268 (=R136) and was contained within the largest SWS aperture, while the long slit of T03 fell about 20–30 arcsec to the west, missing the 20×33-arcsec^2 SWS aperture and passing through the multiple stars R139 and R140[2] in an approximate NE–SW direction. From a comparison of the intensities of eight H I lines (Brα, Brβ and Pf$\alpha - \zeta$) listed by Vermeij et al. (2002) with the theoretical recombination-line ratios by Storey & Hummer (1995), the estimated Hβ flux, corrected for interstellar extinction, falling into the 14×20-arcsec^2 SWS aperture is 1.27×10^{-10} erg cm^{-2} s^{-1}. The line fluxes between 12 and 180 µm from Vermeij et al. (2002) were scaled down by factors of 1.35 (SWS, 12–27.5 µm), 2.35 (SWS, 27.5–45.2 µm) and 7.35 (LWS, 45–180 µm), based on the relative sizes of the four rectangular SWS apertures and the need for flux continuity in the spectral continuum, and then cast in units relative to Hβ. Regarding UV data, the de-reddened intensity of C III] $\lambda 1909$ is from observations in the years 1979–80 (Dufour, Shields & Talbot Jr 1982), and was adopted instead of more recent *HST* observations by Garnett et al. (1995a) taken through the 1-arcsec FOS circular aperture. The 10×20-arcsec^2 elliptical aperture of the *IUE* was centered on a position roughly identical to that targeted by the SWS. We used the measured line strengths, relative to $\lambda 1909$, by Garnett et al. (1995a) for the O III] $\lambda 1666$ and N III] $\lambda 1750$ intensities (which are therefore tentative only), while the Si III] $\lambda\lambda 1883$, 1892 fluxes were from the $F(\mathrm{Si\,III])}/F(\mathrm{C\,III]})$ ratio measured by Garnett et al. (1995b) with the FOS.

The heavy-element ORLs utilized in this work include the C II $\lambda 4267$ line and the multiplets N II $\lambda 5679$ (V3), O I $\lambda 7773$ (V1), O II $\lambda 4075$ (V10), O II $\lambda 4340$ (V2) and O II $\lambda 4650$ (V1) [co-added intensities; standard theoretical relative line ratios were used to estimate unobserved multiplet components where necessary; see e.g. Liu et al. (1995), Liu et al. (2000) and Tsamis et al. (2004)]. Upper

limits were adopted for the undetected N II $\lambda 4041$, Ne II $\lambda 4392$ and Mg II $\lambda 4481$ lines.

For this study, the adopted total de-reddened Hβ intensity from 30 Doradus is 1.19×10^{-8} erg cm^{-2} s^{-1}, in line with the aforementioned Hα estimate by Kennicutt & Hodge (1986) for the central 30 arcmin; the adopted logarithmic reddening constant was $c(\mathrm{H}\beta) = 0.44$. T03 and Vermeij et al. (2002) found values of 0.41 and 0.48 from fixed long-slit and drift-scan slit spectra, respectively. These estimates compare favourably with a mean extinction of about 0.5 dex derived from Hα/Hβ ratio maps of the central 6×6-arcmin^2 region by Lazendic et al. (2003). The optical-line intensities listed in Table 3 are essentially taken from P03, who de-reddened the fluxes using $c(\mathrm{H}\beta) = 0.92$ (the maps of Lazendic et al. (2003) do indicate higher than average extinction at the position observed by P03). The NTT long-slit spectra of T03, which sampled a more extended 'slice' of the nebula, were consulted for consistency checks. The UV, IR and radio fluxes, although carefully calibrated relative to Hβ, do not necessarily sample exactly the same emission regions targeted by the optical observations.

3 PHOTOIONIZATION MODELLING

3.1 The code

The modelling is undertaken using the detailed photoionization code NEBU (e.g. Péquignot et al. 2001) in which the radiative transfer is computed using the outward-only approximation along 20 directions in spherical symmetry, and the ionization state and plasma temperature are determined by solving the relevant equilibrium equations. A model is built by combining a user-defined number of sectors extracted from different spherically symmetric models sharing the same central source of primary ionizing radiation, each with its own covering factor $\omega/4\pi$ of the source, radial hydrogen-density distribution $N_\mathrm{H}(r)$, gas filling factor ϵ, and a set of elemental abundances relative to hydrogen. The code version used here does not include an interstellar dust component.

3.2 Modelling strategy

3.2.1 The 'average filament'

30 Doradus is much larger than R136 and can be viewed as a gaseous shell photoionized by a point-like source located at the centre of an inner cavity. Published images reveal the complex, frothy appearance of the nebula, whose overlapping loops, arcs, and shells are believed to have originated in interacting stellar-wind outflows and expanding SNRs (e.g. see the 3- and 6-cm radio and Hα, Hβ images by Lazendic et al. 2003, and references to imaging and kinematical studies therein). The mean square root electron density $\langle N_e^2 \rangle^{\frac{1}{2}}$ of 30 Doradus, derived from the Hβ flux of the central 30 arcmin under the assumption of a uniformly filled sphere, is two orders of magnitude smaller than the N_e derived from the [O II] and [S II] doublet ratios. This indicates that the bulk of the emission arises from a small fraction of the total volume, as suggested also by the highly filamentary appearance of the nebula. This common feature of GHIIRs is often handled with the concept of a 'filling factor', ϵ. In the classical form of this concept, the emitting gas is assumed to belong to *infinitesimal*, optically thin clumps distributed more or less uniformly between an inner and outer radius, and occupying altogether a fraction ϵ of the nebular volume (e.g. Osterbrock 1989). In this approximation, which aims at emphasizing the observed geometrical extent of the HIIR, the high-excitation gas generally lies close to the energy source whereas the lower excitation gas is found farther

---

[2] Both R139 and R140 contain WR components; see their spectrograms by T03.

out. This is usually not borne out by observation: although shallow radial gradients may exist throughout the nebula, filaments tend to emit both high- and low-ionization lines at whatever distance from the ionizing source.[3] The very existence of a filamentary structure contradicts the classical concept. As confirmed by photoionization modelling, given the primary ionizing flux and the gas density of 30 Doradus, matter becomes optically thick to ionizing radiation over distances which are much smaller than the nebula and similar to the typical thickness of the observed filaments (e.g. compare the spatial thickness of the model nebula with its radius in Table 2). Large-scale radial gradients, if present, are likely due to a global variation of the ionizing parameter with position, for example, in the case that the average density of the different filaments does not scale as the inverse square of their distance from the ionizing source.

As an alternative to the classical description, we consider *macroscopic*, essentially radiation-bounded filaments which are distributed throughout the nebula. Each one of them produces a radially extended shadow, which emits much less than the filament itself since it is subjected only to the weak, extremely soft, diffuse field from other filaments. Here, this alternative description is adopted in its simplest first approximation, namely, in terms of one representative 'average filament'. Given its small geometrical thickness, the radial structure of the filament can be treated assuming spherical symmetry without loss of generality. As a matter of fact, the adopted geometry enters only in the computation of the diffuse field, and there only to a limited extent since the diffuse field is either relatively unimportant in the limiting case of small opacity/optical depth, or very local (i.e. fully independent of geometry) in the opposite limiting case. Depending on the overall covering factor of the entire set of filaments, ionizing radiation may or may not leak out from the nebula. In this work, it is assumed that the overall covering factor is unity, and the power of the ionizing source is the one inferred from the integrated Hα emission over 30 arcmin, that is, a large fraction of the total emission. This amounts to computing the emission of a fully spherical, geometrically thin shell with no escape of the primary and diffuse field. Adopting the spectrum secured by P03 as representative of the whole nebula simply means that the properties of our 'average filament' will be somehow weighted by the regions effectively observed.

3.2.2 Model parameters

Computations are therefore done assuming a smooth small-scale density distribution, that is, a gas filling factor of unity. The pair of (T_e, N_e) varies according to the following general law for a variable gas pressure P, given here as a function of the radial optical depth, τ, at 13.6 eV:

$$P(\tau) = \frac{P_{in} + P_{out}}{2} + \frac{P_{out} - P_{in}}{\pi} \tan^{-1} \left[\kappa \log \left(\frac{\tau}{\tau_\kappa} \right) \right]. \quad (1)$$

The pressure is related to the gas temperature and density via the ideal gas law. At the first step of the computation ($\tau = 0$) the initial pressure is P_{in}, while at the last step ($\tau = \infty$; in practice $\gg 1$) the final pressure is P_{out}. Equation (1) introduces three free parameters in the modelling process: P_{in}, P_{out}, and the optical depth at which the transition from inner to outer pressures occurs (τ_κ). The 'slope' of this transition is controlled by κ, which is arbitrarily taken as $\kappa = 10$, ensuring a smooth transition in all computations presented

---

[3] This is indicated from an analysis along ∼150 arcsec of the slit of T03 which was placed roughly along the radial direction of the nebula and crossed several filamentary nebulosities (cf. fig. 5 of that paper).

here. In practice, τ_κ will have almost the same value 3.4 ± 0.1 in all computations and the gas distribution is controlled by two free parameters, P_{in} and P_{out}, along with the inner nebular radius. The realistic picture of a filament core surrounded by a dilute halo or envelope dictates that $P_{in} < P_{out}$. The adopted pressure law proved to be a convenient tool for the exploration of the effects of the density distribution on the model constraints and predictions; for example, P_{in} could be constrained by the [O III] 52-μm/88-μm line ratio and/or the [O III] λ5007/52-μm ratio, or else some ionization-balance consideration (e.g. [Ar IV]/[Ar III]), while P_{out} was constrained by the [O II] λ3726/λ3729 ratio.

Either a blackbody (BB) or a model stellar-atmosphere spectrum was used to simulate the spectral energy distribution (SED) of the primary ionizing source. The *CoStar* model stellar atmospheres (Schaerer & de Koter 1997), which include non-local thermodynamic equilibrium (LTE) treatment, line blanketing and stellar-wind effects, were adopted. The central source was controlled by a luminosity L and a temperature T_{eff}. For the BB models, a scaling factor δ was applied to the flux at $\geqslant 4$ ryd in order to fit He II λ4686 (from T03). Given the very small amount of radiative energy involved here, δ is of negligible consequence for any other output or prediction of the model ($\delta \simeq 0.10$ in adopted models). For the *CoStar* models, additional parameters would be (i) the metallicity of the stellar atmosphere, taken to be the metallicity of the LMC, and (ii) the luminosity distribution of stars in the central cluster. Since our aim was not to realistically model any particular stellar cluster but only to evaluate the consequences of varying the primary SED within reasonable limits (i.e. BB versus *CoStar*), stars with luminosity of 10^{39} erg s^{-1} were systematically adopted here, with their number defining the total luminosity of the source.

In summary, there are 17–18 basic line intensities and intensity ratios which constrain an equal number of model parameters: that is, the reddening correction; two or three central-source parameters (L, T_{eff}, δ); three nebular parameters (R_{in}, P_{in}, P_{out}); and 11 elemental abundances relative to hydrogen – see Table 1. All other UV, optical and IR observables (Table 3) were treated as 'model predictions', whose relevance was evaluated in terms of the employed atomic data, the observational (and calibration) uncertainties, as well as more general astrophysical considerations.

Table 1. Model parameters and observational constraints.

Parameter	Constraint (flux or flux ratio)
$c(H\beta)$	Hα/Hβ (taken from P03)
$L_\star$	Absolute flux $I(H\beta)$
T_{eff}	[O III] λ4959 + λ 5007
δ (4 ryd)[a]	He II λ4686 (for BB models only)
R_{in}	[O III] (λ4959 + λ5007)/[O II] (λ3726 + λ3729)
P_{in}	[O III] 52 μm/88 μm or [Ar IV]/[Ar III]
P_{out}	[O II] λ3726/λ3729
He	Mean of He I λλ4471, 5876
C	C III] λ1908
N	[N II] λ6548 + λ6584
O	[O III] λ4363/(λ4959 + λ5007)
Ne	[Ne III] λ3869 + λ3968
Mg	Mean of Mg I] λλ4562, 4571
Si	Mean of Si III] λλ1883, 1892
S	Mean of [S III] λλ6312, 9069, 9532
Cl	Mean of [Cl III] λλ5517, 5537
Ar	[Ar III] λ7135 + λ7751
Fe	[Fe III] λ4658

[a]Scaling factor of the BB flux at $\geqslant 4$ ryd (see text).

Table 2. Model parameters and physical properties.

| Model	S1	S2	D1 Hydrogen-poor	D1 Normal	Mean	D2 Hydrogen-poor	D2 Normal	Mean
Primary spectrum	*Planck*	*CoStar*[a]		*Planck*			*CoStar*[a]	
Effective temperature, T_{eff} (kK)	49.3	37.6		51.6			38.0	
Luminosity, L (10^8 L$_\odot$)	1.12	1.98		1.08			1.90	
Inner radius, R_{in} (10^{19} cm)	7.80	10.15		8.25			10.50	
Thickness (10^{18} cm)	8.39	5.07		8.23			2.87	
P_{in} (10^{-10} CGS)	4.16	4.16		4.00			6.00	
P_{out} (10^{-10} CGS)	12.20	12.40		11.1			11.4	
Covering factor, $\omega/4\pi$	1.00	1.00	0.080	0.920	1.00[b]	0.086	0.914	1.00[b]
Filling factor, ϵ	1.00	1.00	0.105	1.000	–	0.072	1.000	–
Inner $N(H^+)$ (cm^{-3})	140	145	343	136	–	614	211	–
$\langle N_e \rangle$ (cm^{-3})	201	204	440	192	198	696	271	279
$\langle T(H^+) \rangle$ (K)	9962	9927	5026	9942	9716	3987	9895	9654
$t^2(H^+)$	0.0045	0.0064	0.0696	0.0054	0.0175	0.0544	0.0072	0.0224
$t^2(O^{2+})$	0.0031	0.0046	0.0386	0.0039	0.0715	0.0338	0.0053	0.0779
τ (13.6 eV)	90	92	29	90	–	9	34	–
Hβ fraction	1.00	1.00	0.081	0.919	1.00[b]	0.084	0.916	1.00[b]
Gaseous mass (10^3 M$_\odot$)	151	149	3.51	144	147[b]	1.96	106	108[b]
He/H	0.0858	0.0854	0.1000	0.0831	0.0835	0.1000	0.0825	0.0828
C/H ($\times 10^5$)	4.33	4.60	66.0	4.63	5.98	72.3	4.96	6.09
N/H ($\times 10^5$)	1.74	1.42	15.3	1.74	1.78	18.8	1.46	1.75
O/H ($\times 10^5$)	22.90	23.20	200.0	24.40	28.30	200.0	25.40	28.30
Ne/H ($\times 10^5$)	4.33	4.00	44.0	4.52	5.39	60.0	4.38	5.31
Mg/H ($\times 10^7$)	52.0	39.5	200.	50.8	54.7	280.	40.0	44.3
Si/H ($\times 10^7$)	25.2	28.0	35.	28.5	28.6	217.	31.0	34.0
S/H ($\times 10^7$)	61.0	68.0	84.	68.0	68.4	455.	65.0	71.4
Cl/H ($\times 10^7$)	0.59	0.69	0.8	0.66	0.66	5.0	0.72	0.79
Ar/H ($\times 10^7$)	12.0	12.6	16.	13.1	13.2	92.	13.2	14.5
Fe/H ($\times 10^7$)	11.7	11.0	17.	13.7	13.8	81.	11.6	12.7
Y	0.253	0.252	0.274	0.247	0.248	0.273	0.246	0.246
Z	0.005	0.005	0.036	0.004	0.005	0.040	0.004	0.006

[a]Stellar-atmosphere model of 10^{39} erg s^{-1} luminosity and typical LMC metallicity. [b]Sum of components instead of mean.

3.3 Chemically homogeneous models

We initially constructed single-component, chemically homogeneous models. Adopted parameters and derived physical conditions for two of these – referred to as S1 and S2 (with a BB and a *CoStar* ionizing spectrum, respectively) – are listed in Table 2. Chemically inhomogeneous, dual-component models D1 and D2 are introduced in Section 3.4. The models are radiation bounded (optical depths at the end of each computation are given in Table 2). *CoStar* models have a larger inner radius and a smaller spatial thickness, driven by the need to lower the ionization state of the gas which was otherwise overestimated, as judged from the ionization balance of oxygen mainly, due to the increased hardness of the primary spectrum. The density profile of model S1 is quite similar to the profile of the normal-abundance component of model D1 (Section 3.4) plotted in Fig. 1. The ratios of predicted over observed line intensities (hereafter the 'departure ratios') are listed in Table 3 (columns 4 and 5) and the overall quality of the fit (i.e. closeness to unity) can be judged from those.

3.3.1 Comments

Models S1 and S2 provide us with a view of the influence of the primary spectrum on the predictions. To first order these models were successful in that it was possible to generate a set of parameters fulfilling all basic requirements of Table 1, while many predictions compare well with observation (Table 3). Many of the unsatisfactory
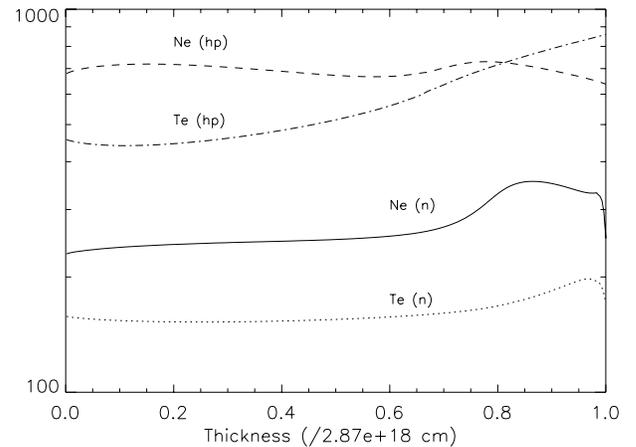
Figure 1. Electron-density distribution, N_e, and temperatures T_e (scaled down to 0.02 and 0.14T_e, respectively, for the normal 'n' and hydrogen-poor 'hp' phases) of the dual-abundance model D2.

departure ratios correspond to poorly determined line intensities or upper limits. This overall agreement suggests that basic assumptions are quite acceptable, while the atomic data and the observations used are generally quite accurate. A commentary on remaining discrepancies is of interest in order to evaluate their significance and determine the *astrophysical* relevance of the chemically homogeneous description. Also, many features of S1–S2 are common with

Table 3. Comparison of predictions from models S1, S2, D1 and D2. The observed, de-reddened intensities are in units such that $I(H\beta) = 10^3$, except the radio-continuum fluxes whose units are Jy; the model predictions are given as the ratio of predicted over observed values in each case.

Line	λ (Å)[a]	I_{obs}^b	S1	S2	D1	D2
Hydrogen and helium recombination lines, optical and radio continua
Hβ	4861.3	1000[c]	1.00	1.00	1.00	1.00
Hα	6562.8	2850	1.02	1.02	1.02	1.02
Hγ	4340.5	483	0.97	0.97	0.97	0.97
He I[d]	3187.7	27.4	1.05	1.06	1.06	1.03
He I (B)	3613.6	4.02	1.28	1.27	1.24	1.22
He I	3888.6	51.7	1.00	1.00	1.00	1.00
He I (B)	3964.7	8.61	1.23	1.22	1.19	1.18
He I	4026.2	21.5	0.94	0.94	0.92	0.92
He I	4120.8	2.60	0.73	0.73	0.70	0.69
He I	4387.9	5.50	0.96	0.96	0.95	0.94
He I (B)	4437.6	0.565	0.81	0.81	0.78	0.77
He I	4471.5	43.1	1.01	1.01	1.00	1.00
He I	4713.2	4.81	1.12	1.11	1.06	1.05
He I	4921.9	11.31	1.01	1.01	1.00	1.00
He I (B)	5015.7	22.04	1.22	1.22	1.19	1.17
He I	5875.7	121.2	1.00	1.00	1.00	1.00
He I	6678.2	33.85	0.99	0.99	1.00	1.00
He I	7065.2	28.30	1.76	1.75	1.62	1.66
He I (B)	7281.3	4.52	1.42	1.41	1.37	1.35
He II	4686.0	0.171	1.00	1.54	1.00	1.88
BJ/Hβ	3646	4.53	0.97	0.98	1.03	1.06
Continuum	1.40 GHz	37.6	1.05	1.06	1.03	1.02
Continuum	2.45 GHz	37.0	1.04	1.04	1.02	1.00
Continuum	4.75 GHz	35.8	1.02	1.01	0.99	0.98
Continuum	4.85 GHz	36.0	1.01	1.00	0.98	0.97
Continuum	8.55 GHz	34.8	0.98	0.98	0.96	0.94
Heavy-element recombination lines
[C I]	9850.3+	0.276	0.37	0.34	0.84	0.66
C II	4267.2	0.919	0.43	0.42	1.00	1.00
N II	4038.0	<0.1	0.53	0.39	0.83	0.86
N II	5679.0+	0.186	0.71	0.52	1.00	1.00
O I	7773.0+	0.124:	0.58	0.55	1.58	1.85
O II	4075.0+	3.05	0.62	0.63	0.97	0.97
O II	4341.0+	1.54	0.69	0.70	1.05	1.05
O II	4651.0+	3.70	0.66	0.68	1.01	1.01
Ne II	4394.0	<0.2	0.44	0.44	0.74	0.65
Mg II	4481.2	<0.1	0.50	0.37	0.61	0.55
CELs (UV and optical)
C II]	2322+	70:	0.67	0.86	0.65	0.79
[O III]	+2321	–	–	–	–	–
C III]	1907+	150	1.00	1.00	1.00	1.00
C IV	1549	12:	0.31	0.83	0.37	0.69
[N I]	5197.9	1.29	0.28	0.27	0.33	0.16
[N I]	5200.2	0.693	0.56	0.53	0.64	0.29
[N II]	5754.6	1.87	1.08	1.10	0.88	0.98
[N II]	6583.5+	152	1.00	1.00	1.00	1.00
N III]	1744 +	<15	0.76	0.59	0.61	0.56
[O I]	6300.3+	12.5	1.05	2.20	1.37	1.04
[O II]	3726.1	586	1.00	1.00	1.00	1.00
[O II]	3728.8	637	1.00	1.00	1.00	1.00
[O II]	7319.8+	37.3	0.93	0.96	0.89	0.96
[O III]	1663	15:	2.16	2.19	2.18	2.20
O III]	4363.2	32.1	1.00	1.00	1.00	1.00
[O III]	5006.8+	6790	1.00	1.00	1.00	1.00
[Ne III]	3869.1+	444	1.00	1.00	1.00	1.00
Mg I]	4562.6	0.716	1.05	1.06	1.06	1.05
Mg I]	4571.1	0.617	0.94	0.94	0.94	0.95
Si III]	1882.7	20.6	1.04	1.04	1.04	1.05
Si III]	1892.0	14.4	0.96	0.96	0.96	0.97

Table 3 – *continued*

Line	λ (Å)	I_{obs}	S1	S2	D1	D2
[S II]	4068.6	8.71	0.77	1.37	0.82	1.03
[S II]	4076.3	2.95	0.74	1.31	0.79	0.98
[S II]	6716.4	71.2	0.68	1.19	0.74	0.90
[S II]	6730.8	65.6	0.65	1.13	0.70	0.87
[S II]	10 320.0+	6.6:	0.90	1.60	0.96	1.20
[S III]	6312.0	18.1	0.79	0.80	0.78	0.75
[S III]	9530.6+	938	1.08	1.09	1.08	1.09
[Cl II]	8578.7+	0.76:	1.04	1.58	1.08	1.64
[Cl III]	5517.7	4.49	1.00	1.00	1.00	0.99
[Cl III]	5537.7	3.32	1.00	1.00	1.00	1.01
[Cl III]	8433.7+	0.250	0.99	1.00	0.99	0.99
[Cl IV]	8045.6+	0.494	2.58	4.79	3.08	3.92
[Ar III]	5191.8	0.663	1.38	1.38	1.36	1.34
[Ar III]	7135.8+	148	1.00	1.00	1.00	1.00
[Ar IV]	4711.4	1.31	2.55	3.97	2.99	3.14
[Ar IV]	4740.2	0.986	2.52	3.92	2.95	3.13
[Fe II]	5158.8	0.306	1.12	1.78	1.36	1.39
[Fe II]	7155.2	0.207	0.78	1.21	0.93	1.07
[Fe III]	4008.3	0.284	0.81	0.82	0.79	0.81
[Fe III]	4658.2	4.89	1.00	1.00	1.00	1.00
[Fe III]	4701.5	1.25	0.98	0.99	0.99	0.99
[Fe III]	4733.9	0.405	0.88	0.88	0.89	0.89
[Fe III]	4881.1	1.51	0.74	0.74	0.73	0.74
[Fe III]	4924.7	0.341	0.66	0.66	0.67	0.67
[Fe III]	5270.5	2.44	1.01	1.01	1.02	1.02
[Fe IV]	6734.4	0.228	1.72	1.52	1.87	1.44
CELs (IR)
[N II]	121.8 μm	<2.7	0.86	0.86	1.20	1.31
[N III]	57.3 μm	104	1.51	1.10	1.67	1.36
[O III]	51.8 μm	1330	1.06	1.08	1.40	1.34
[O III]	88.3 μm	1250	1.07	1.08	1.29	1.07
[Ne II]	12.8 μm	99.0	0.39	0.18	1.05	0.79
[Ne III]	15.6 μm	650	0.91	0.91	1.22	1.41
[Ne III]	36.0 μm	65.0	0.81	0.80	1.07	1.21
[S III]	18.7 μm	320	1.05	1.05	1.13	1.53
[S III]	33.5 μm	550	0.82	0.81	0.87	1.04
[S IV]	10.5 μm	600	1.62	1.93	1.83	1.59
[Ar II]	6.98 μm	2.4:	0.94	1.43	1.03	1.83
[Ar III]	8.99 μm	115	0.95	0.95	1.01	1.27
[Ar III]	21.8 μm	11.5	0.65	0.65	0.69	0.85

[a] '+' indicates that predictions are for the total intensity of the multiplet in each case. [b] ':' indicates uncertain flux and '<' an upper limit flux estimate. [c] Fit to de-reddened, total Hβ flux $I(H\beta) = 1.19 \times 10^{-8}$ erg s^{-1} cm^{-2}. [d] '(B)' indicates a prediction for Case B recombination of some He I singlet lines (see text).

the following, more elaborate, models. Optical lines are considered first.

(i) *He* I. The λ7065 line appears overestimated, but can be affected by telluric absorption: this line is 1.5 times stronger in the spectrum of T03. Singlet He I lines were computed assuming Case B recombination (e.g. Osterbrock 1989). Except for the very weak λ4437 line, all of those singlet lines which are much weaker under Case A (they are noted with a 'B' in column 3 of Table 3) are systematically overestimated by the model, indicating that there is some departure from Case B in 30 Doradus. This is possible even in optically thick nebulae since the resonance lines of He I can be absorbed by hydrogen atoms before being converted into optical He I lines, and this misfit has no bearing on either the quality of the observations or the relevance of the model premises. The He I λ4121 misfit is possibly due to the observed line intensity being affected

by blending with O II V20 multiplet lines other than λ4119.22 listed by P03. The perfect fit to λ3888 was obtained partly, thanks to a secondary parameter, namely, an average 'He$^+$ turbulent temperature', which is introduced to modulate somewhat the optical depth in the 2^3S–n^3P transitions, and is proportional to the column density of the 2^3S metastable level [concerning the He I triplet transfer, see e.g. Osterbrock (1989)]. The validity of this description and the quality of the observations can be appreciated from (i) the good fit to λ3187, also sensitive to optical depth, and (ii) the fact that the adopted He$^+$ turbulent temperatures (6, 3, 4 and 5 × 10^4 K for S1, S2, D1 and D2, respectively) are very reasonable.

(ii) *Low-ionization lines.* Inspection of Table 3 shows that emission from low-ionization species, such as [O I] λλ6300, 6363, is rather well fitted even though model S2 overestimates the [O I] flux by ∼0.3 dex. An overestimation of [O I] may suggest that, contrary to our assumption, the material is not strictly radiation bounded along all radial directions. It may also indicate that too many 'hard' photons arise from the source and are eventually absorbed at the ionization front (see also the commentary on [Ar IV] below). On the other hand, emission of the [N I] λ5200 multiplet and the [S II] lines is underestimated by 0.7 and 0.3 dex, respectively, in model S1. *CoStar* model S2 reproduces the [S II] flux much better, without improving the fit to the [N I] lines. Note the overall agreement of the [S II] relative line intensities. The intensity of the far-red [S II] multiplet was based on the strongest line [S II] λ10320, re-calibrated by means of the three strongest neighbouring H I and He I lines, which consistently point to an upward correction of the intensities by a factor of 1.28 in this wavelength range of the VLT spectrum (in this range, lines with de-reddened intensities less than 0.1 in the present units lead to inconsistent results). The collision strengths for [N I] are questionable as recent results by Tayal (2000) inexplicably differ from previous ones by as much as one order of magnitude. Here, the values obtained by Berrington & Burke (1981) were used. A small wavelength interval including [N I] λ5200 was unfortunately not observed by T03.

Finally, the [C I] λ9850 line is to a large extent excited by recombination (∼50 per cent on an average for the whole nebula). The fact that it is underpredicted is to be considered in connection with the poor fit to the heavy-element ORLs (see below), even though the line can also arise from the photodissociation region (PDR), which emits lines like the strong [O I] 63 μm and is not modelled here.

(iii) *High-ionization lines.* All models, S2 especially, overestimate the emission of [Ar IV] and probably also [Cl IV] (the latter line is weak). The recombination coefficients for these species are poorly known, and the adopted approximate empirical values were derived from an unpublished model of the PN NGC 7027 by Péquignot. For example, the empirical coefficient is eight times the radiative coefficient in the case of Ar^{3+} recombination. The mean fractional concentrations of Ar^{+3} and Cl^{+3} are moderate (∼8 and 13 per cent in model S1; ∼11 and 21 per cent in model S2), and very sensitive to density as these are the highest ions present in the gas. While line fluxes by P03 and T03 are generally in fair agreement, the [Ar IV] lines are striking exceptions, with the fluxes of T03 about 70 per cent larger, suggesting that (i) the concentration of Ar^{+3} indeed varies greatly with position in the nebula and consequently (ii) an overestimation of these line fluxes not exceeding ∼0.3 dex in a model is probably not physically significant. From trials it was found that BB models at constant densities ($N_e = 300$ cm^{-3}) overestimate the [Ar IV] and [Cl IV] fluxes by ∼50 per cent only, whereas *CoStar* models with a positive radial density gradient overestimate this flux by up to 0.60 dex (model S2). The latter discrepancy would tend to invalidate the prominent continuum flux excess (relative to

a BB of the same T_{eff}) shown for $h\nu > 40$ eV by the *CoStar* stellar atmospheres, in the way they were used here. Also, the extended, low-density halo of the high-excitation zone of our model filament was tailored to fit the [O III] far-infrared (FIR) ratio (models S1–S2). The 80-arcsec LWS lobe, however, sampled a large area in which the mean density may be predictably lower than the one called for by the [Ar IV] UVES ratio; UVES sampled a small bright filamentary region whereas LWS targeted an area of lower average surface brightness [see fig. 2 of Vermeij et al. (2002)]. These discrepancies are therefore understood in terms of conflicting density sampling of the IR and optical density-sensitive ratios due to the different spatial coverage of each spectral domain, and of the uncertainty regarding the exact shape of the primary continuum at high energies (see also model D2 in Section 3.4).

(iv) *Intermediate-ionization lines.* The [S III] auroral λ6312 and nebular λ9069 and λ9532 lines are imperfectly matched. The relative intensity ratio of the nebular lines agrees with theory within 8 per cent (Mendoza 1983), although these lines are often affected by telluric absorption; considering this agreement and their large strength, more weight was given to them than to λ6312 in the determination of S/H abundance ratio. Calculations were performed here using the collision strengths by Galavis, Mendoza & Zeippen (1995) for [S III], [Ar III] and [Cl IV], who devoted particular attention to the fine-structure lines and then argued that the [Ar III] results were not controversial (Galavis, Mendoza & Zeippen 1998). The collision strengths for [S III] may not be of ultimate accuracy however: in a trial calculation using the data published by Tayal & Gupta (1999), all three optical [S III] lines were almost exactly matched using the previously determined S/H abundance ratio.

The [N II] λ5755 line is some 10 per cent high in both sulphur models, pointing to a possible weakness of these chemically homogeneous models (see Section 3.4). Here the presumably accurate collision strengths by Hudson & Bell (2005) were adopted.

(v) *CNO ORLs.* The ORLs of CNO are systematically underpredicted. This is the *raison d'être* of the present study (Sections 3.3.2 and 3.4).

(vi) *IR lines.* The computed fine-structure ratios for the [Ne III] and [Ar III] transitions are not sensitive to model assumptions in the conditions of 30 Doradus, and the imperfect match of these ratios cannot be taken as an inadequacy of the astrophysical assumptions themselves. Whatever the cause, these discrepancies suggest that a mismatch of ∼15 per cent for other fine-structure line ratios might not be significant. The discrepancy is larger for [Ar III], but [Ar III] 21.8 μm is one of the weakest IR lines. It is found from both S1 and S2 models that the predicted [Ne III] 15.6- and [O III] 51.8-μm line fluxes support a higher Ne/O abundance ratio than their optical counterparts do (if only by 15–18 per cent). In this regard, these homogeneous models fail to exactly fit the optical and IR neon and oxygen lines simultaneously. In contrast, the S1–S2 models differ significantly for [N III] 57 μm, with the *CoStar* computation leading to much more consistent results. The collision strengths used for [N III] in these computations are from Stafford, Bell & Hibbert (1994). Were we to use the larger values obtained previously by Blum & Pradhan (1992), the difficulty met with [N III] in BB models would be exacerbated. None the less, the most obvious failure of these models is the underprediction of [Ne II]. The IR lines are reconsidered in Section 3.4.2

3.3.2 Two-sector models

Chemically homogeneous models comprising two sectors were also investigated. The idea (which has been tried in the past) was to

check whether the different mean densities of the two model sectors would induce significant global temperature variations and whether this would result in a better fit for the CNO ORLs. A simple approach was taken by using the same smooth scale-density law for both sectors, but imposing different densities (by a factor of 2) at the innermost point of each. Vastly different starting values were not supported by the observed density-line ratio diagnostics. The model fitting was as good as for model S1 with the same abundances for all elements. The fit to the heavy-element ORLs did not improve at all however (e.g. C II $\lambda4267$ still underestimated by 0.3 dex). The electron-temperature difference between the two components amounted to 120 K while the mean density differed by a factor of ~2. Resulting global temperature-fluctuation parameters for representative ions were $t^2(\mathrm{H}^+) = 0.0038$ and $t^2(\mathrm{O}^{2+}) = 0.0026$. Similar low-$t^2$ factors were reported by Kingdon & Ferland (1995) who investigated chemically homogeneous models incorporating a much broader range of density variations.

3.3.3 Ionizing-spectrum characteristics and model radii

The Ly-c ionizing flux of model S1 is 7.55×10^{51} photon s^{-1}, comparable to the Ly-c flux of 4.2×10^{51} photon s^{-1} derived by Crowther & Dessart (1998) emanating from within a 10-pc radius from the massive core cluster R136, or that of $\sim1.2 \times 10^{52}$ photon s^{-1} obtained by Israel & Koornneef (1979) for the inner 3×3 arcmin^2 (45×45 pc) of the nebula. By construction, the total Hβ flux computed by the model fits the measurement of Kennicutt & Hodge (1986) with a circular 30-arcmin aperture (i.e. a physical radius of ~218 pc). The absolute radio fluxes are also well accounted for since the effective beam sizes used in the radio observations of Filipovic et al. (1995) are contained within the above 30-arcmin aperture.

Regarding the shape of the ionizing spectrum, the BB temperature of 49.3 kK corresponding to model S1 falls within the T_{eff} range of 43–51 kK derived by Martín-Hernández et al. (2002) from the known, observed 30 Doradus stellar spectral types using the T_{eff} – spectral-type calibrations of Vacca, Garmany & Shull (1996) and Martins, Schaerer & Hillier (2002). The T_{eff} obtained using the *CoStar* stellar-atmosphere models, however, is 37–38 kK only, again in excellent agreement with the findings of Martín-Hernández et al. (2002) who used those models and the CLOUDY photoionization code to derive the stellar properties of 30 Doradus from the same *ISO* observations that were used in this work.

The outer radii of these models span a range of 27–35 pc (Table 2), equivalent to 111–144 arcsec. This is in very good agreement with the actual position of the UVES slit at a *projected* distance of 88 arcsec from R136. Furthermore, the derived thickness of our 'average filament' is 2–3 pc corresponding to 8–12 arcsec at 50 kpc. The filament of model D2 (Section 3.4) is thinner being roughly 1 pc wide (see Fig. 1). Inspection of the Hβ image of the nebula presented by Lazendic et al. (2003) shows that the UVES slit fell on a prominent filament with an apparent width of about 8 arcsec. These findings suggest that our approach is successful in as much as, being based exclusively on observed nebular line intensities, the models correctly *predict* both the global ionizing-source properties and the approximate spatial characteristics – distance from R136 and extent – of the region sampled by spectroscopy.

The gas-phase abundances of these chemically homogeneous models are discussed later in Section 3.6 along with our preferred 30 Doradus gaseous abundances. Taking into account the above remarks and the commentary of Section 3.3.1, we find that the majority

of lines, both CELs from heavy elements and H I and He I ORLs, can be reasonably well fitted, with the crucial exception of the CNO ORLs: predictions for these were found to be identical across models, that is, consistently underestimating the observed ORL fluxes (Table 3). The behaviour of these lines under widely different modelling assumptions such as constant or variable gas density, and BB or stellar-atmosphere ionizing spectrum, necessitates a different approach to the modelling process. This is introduced in the following section in the form of a dual-abundance model nebula comprising two sectors across which the elemental abundances (and therefore other properties such as density and temperature also) vary.

3.4 Dual-component chemically inhomogeneous models

Models that comprise two components which are intimately intermixed are now considered. It is assumed that clumps or filaments of relatively hydrogen-poor gas are embedded in the main body of the nebula, which consists of gas of approximately 'normal' LMC composition. It is also assumed that the clumped phase is co-extensive with the hydrogen-rich component. This latter assumption is a simple guess suggested by evidence from the spatial analysis of T03, which revealed a roughly uniform surface-brightness ratio of the C II $\lambda4267$ and O II ORLs to Hβ across a 160-arcsec swathe of the inner 30 Doradus region. Technically, the results of two appropriately defined spherically symmetric computations were combined. In order for a dual-abundance model to be obtained, a small sector of the normal-composition shell was extracted and substituted by a sector of the hydrogen-poor shell to the effect that the combined emitted Hβ flux remained almost unaltered. The gas-filling factor in the main shell was kept at unity, whereas the small filling factor of the hydrogen-poor shell was adjusted so that the geometrical thicknesses of both shells were identical. The assumption of intimate mixing over a scale much smaller than the shell size led to the complementary notion of *equal pressures for both components at similar optical depths*. Given the identical geometrical extents of the two sectors and the identical amounts of radiation they absorbed and re-processed, the total radiation field experienced by both was approximately similar at any optical depth, and the predicted emission from the dual-sector model was very close to the one which would arise from a single-sector model with many small hydrogen-poor clumps uniformly embedded in the normal-abundance gas throughout the whole shell. The pair of (T_e, N_e) values varied along the radial direction throughout both components according to a $P(\tau)$ law similar to that adopted for the single-component models (Fig. 1).

We consider two representative models: D1 which is built under a BB SED and has fully radiation-bounded components, and D2 which is built under a *CoStar* SED. D2 was tentatively fine tuned to fix the [O I] excess of S2, by considering a large, but finite optical depth in the normal component (Section 3.3.1). The 'one-filament approximation' is obviously coarse and the adopted model filament must be seen as a best compromise. Specifically, for $P_{\mathrm{in}} \lesssim P_{\mathrm{out}}/4$, the [Ar IV] lines become unacceptably strong, even with the proviso of Section 3.3.1, while for $P_{\mathrm{in}} \gtrsim P_{\mathrm{out}}$, [O III] 88 and [S III] 33 μm become too weak compared to [O III] 52 and [S III] 18 μm, respectively (see Section 3.4.2). Accordingly, $P_{\mathrm{in}} \sim P_{\mathrm{out}}/2$ was adopted in model D2. Other models with $P_{\mathrm{in}} \sim P_{\mathrm{out}}/3$ gave more weight to the IR [O III] ratio. Models D1–D2 should be considered in comparison to their respective, one-component counterparts, S1–S2.

3.4.1 Constraining the metallicities of the model components

For an increasing metallicity of the clumped component, its electron temperature decreases due to more efficient cooling from CELs

while, because of the equal pressures, the electron density proportionally increases. The higher density of the hydrogen-poor gas favours N^{2+} and O^{2+} recombination which produces N^+ and O^+. H^0 and He^0 are also enhanced there assisting in the charge-exchange process with O^{2+} and N^{2+} which produces extra singly ionized species (Fig. 3) and boosts the overall efficiency of O I relative to O II ORL emission. The observed intensity of the very weak O I $\lambda 7773$ ORL being rather uncertain, an underestimation of the line may not be significant, although a substantial overestimation is. O I $\lambda 7773$ therefore provides an upper limit to the O/H abundance ratio for the posited clumped phase. On the other hand, for an O/H abundance ratio significantly less than this upper limit, the hydrogen-poor phase heats up and the collisional excitation of [N II] $\lambda\lambda 6548, 6584$ increases selectively due to the low excitation energy of the lines. These two occurrences can help us to bracket the abundances of the posited hydrogen-deficient regions (see also Section 3.4.2).

Regarding model D1, the Si–Fe abundances of the clumped component were kept approximately equal *by mass* to those of the normal component, while those of CNONeMg were enhanced. The ratio of oxygen mass fraction (relative to hydrogen) of the two components is $m^1_O/m^2_O = [(O/H)_1/(O/H)_2](\mu^1_H/\mu^2_H)^{-1}$, where O/H denotes abundance ratio by number and μ^i_H is the mass per gram of hydrogen. For model D1, $(O/H)_1 = 2 \times 10^{-3}$ was adopted after trials and $m^1_O/m^2_O = 7.6$ was found. Then the CNONeMg abundances in the clumps were adjusted iteratively until the observed intensities of the ORLs were matched and without violating the adopted upper limits in the case of undetected lines. The resulting ratios for the CNNeMg mass fractions are 13.1, 9.5, 9.0 and 4.1 (the latter arbitrary), respectively. Thus, the hydrogen-poor phase of D1 has mass fractions of $X = 0.690$, $Y = 0.274$ and $Z = 0.036$.

For model D2 the abundances of Mg–Fe were adopted to be seven times larger in the hydrogen-poor component than in the 'normal' one; this enrichment factor is close to that found for oxygen. Evidence in favour of enhanced Si–Fe in the hydrogen-poor component is presented in Section 3.4.2 The resulting mass fractions of the hydrogen-poor phase in model D2 are $X = 0.687$, $Y = 0.273$ and $Z = 0.040$.

Considering a more extreme enrichment of the clumped phase in heavy elements, a model where the O/H abundance ratio in the metal-rich component was 50 times higher than in the normal phase of model D1 (with Mg–Ar abundances equal by mass in both components), led to much overestimated O I $\lambda 7773$ emission (by 0.85 dex), but to a Balmer jump approximately equal to that observed. A variant of this with Mg–Ar abundances also enhanced by 50 times relative to those in the normal phase, overestimated the Balmer jump by 23 per cent, and resulted in much overestimated total O I $\lambda 7773$ and [Ar II] 6.98-μm line fluxes – by prohibitive factors of ~ 10 and ~ 6, respectively. The fraction of total Hβ flux emitted from the clumps was 4.6 per cent, the clump $T(O^{2+})$ dropped to 978 K, and the mass of the clumped phase was reduced to 254 M$_\odot$. The aforementioned overpredictions for the O I and [Ar II] lines did not improve in trials where the computation involved a density-bounded (as opposed to a radiation-bounded) hydrogen-poor region. We conclude that models where the hydrogen-deficient phase has an oxygen abundance larger than about 10 times (by number) that of the ambient 30 Doradus medium are ruled out.

### 3.4.2 Model predictions

The hydrogen-deficient phase of D1–D2 is of lower ionization compared to the normal phase: there is approximately two times more

H^0 (relative to H^+) and approximately four times more He^0 (relative to He^+) in the clump medium than in the diffuse medium (Table 5). The clumped phase emits only about 8 per cent of the total nebular Hβ flux, but it emits a more significant fraction of [N II] 6548, 6584 Å, [N III] 57 μm, [O III] 52, 88 μm, [Ne III] 15.6 μm and [O II] 3727 Å; up to ~ 30 per cent for the optical and IR nitrogen lines and somewhat less for the oxygen IR lines in model D1. In model D2 about 30–35 per cent of the [Ne III] 15.6-, [S III] 18.7- and [Ar III] 8.99-μm fluxes are emitted from the cool hydrogen-poor component because of its enrichment in neon, sulphur and argon. The flux portion of the C II $\lambda 4267$ line, the O II $\lambda 4650$ V1 multiplet, and each of the He I $\lambda\lambda 4471, 5876$ and 6678 lines emitted from the clumped phase is ~ 58, 32 and 10 per cent of the total, respectively, for both D1 and D2. The relative contributions of each nebular component to the individual emission-line fluxes are shown in Fig. 2 for a representative selection of ORLs, optical/UV CELs and IR CELs in model D2.

Other than the CNO ORLs, inspection of Table 3 shows that the predictions for [C I] $\lambda 9850$ and [Ne II] 12.8 μm are also improved by about 0.3–0.4 and 0.4–0.6 dex, respectively, in models D1–D2 compared to the chemically homogeneous models. The former line is efficiently excited largely by radiative recombination[4] of C^+ in the clumped phase (see also Section 3.3.1), while emission of the latter is favoured by the lower temperature, as well as the five times higher concentration of Ne^+ there (Table 5). The major flux portion of both these lines (~ 60–65 per cent of the total) arises from the hydrogen-deficient inclusions. The He I line spectrum is even better fitted in D1–D2 models (concerning lines sensitive to departure from Case B and $\lambda 7065$, see Section 3.3.1). Notably, due to its partial emission from a cool medium, the predicted flux of the more sensitive to collisional excitation He I $\lambda 4713$ line, is improved by 6 per cent. Main features of the high-excitation lines are as in S1–S2 (Section 3.3.1), with D1 somewhat worse than S1 and D2 somewhat better than S2. On the other hand, D2 is slightly less satisfactory than D1 concerning the fit to the Balmer jump. The interesting case of [N II] is considered below.

The IR CELs merit special attention as they can provide information about the enrichment of neon, sulphur and argon in the posited hydrogen-poor component relative to that obtained for CNO; that is, whether model D2 is to be preferred over D1. Out of 13 IR CELs listed in Table 3, [N II] 122 and [Ar II] 7 μm are extremely weak (or undetected) and their fluxes should be considered uncertain by at least a factor of 2. According to Vermeij et al. (2002), the most uncertain fluxes are those of [S III] 33 and [Ne III] 36 μm, both of which suffer from the uncertain calibration of the SWS-4 detector (by at least 30 per cent); [Ne II] 12.8 μm (25–30 per cent accuracy); and the weak [Ar III] 22 μm. For the purpose of determining the IR calibration self-consistently by comparison to model results, lines which significantly depend on physical conditions should be discarded, and several subsets of IR CELs can be identified (Table 4). In addition to [S III] 33 μm and, particularly, [O III] 88 μm, whose critical densities are low, [S IV] 10.5 μm is also strongly model-dependent in that, analogously with [Ar IV] (Section 3.3.1), it is a high-ionization line sensitive to both the adopted primary spectrum and the density distribution. Thus, an accurate calibration could a priori be based on 'set IR5', comprising the five remaining lines (i.e. IR5: [N III] 57, [O III] 52, [Ne III] 15.5, [S III] 18.6, and [Ar III]

---

[4] The collisional contribution to the line excitation is ~ 35 per cent in the hydrogen-poor component and ~ 50 per cent on an average for the whole nebula.
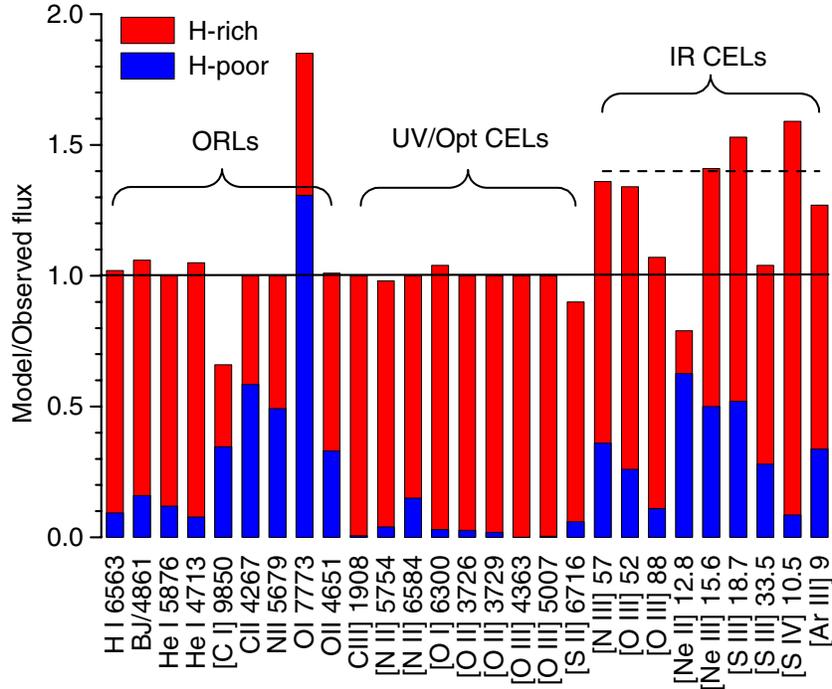
Figure 2. The model over observed flux ratios (departure ratios) for the chemically inhomogeneous model D2 (Tables 2 and 3): the relative contributions of each nebular component to the individual line fluxes are colour coded. Three major groups of lines are identified. [C I] λ9850 is emitted also from the PDR which is not modelled here; O I λ7773 is very weakly observed; the deficit of [O III] 88 and [S III] 33 μm is presumably due to the lines being also selectively emitted by lower density background gas in the *ISO* fields of view. Amongst the IR lines shown, [Ne II] 12.8 and [S III] 33 μm are less accurately measured. The dashed line shows the suggested re-calibration of the IR fluxes relative to the optical (see Section 3.4.2 for details).

Table 4. Average departure ratio and 1σ scatter for IR lines.

Line set	S1	S2	D1	D2
IR4[a]	0.99 ± 0.07	1.00 ± 0.08	1.19 ± 0.13	1.39 ± 0.08
IR5[b]	1.10 ± 0.22	1.02 ± 0.08	1.29 ± 0.20	1.38 ± 0.07
IR7[c]	1.17 ± 0.24	1.16 ± 0.30	1.36 ± 0.21	1.37 ± 0.12
IR11[d]	0.99 ± 0.36	0.96 ± 0.44	1.20 ± 0.28	1.22 ± 0.21

[a]IR4: [O III] 52, [Ne III] 15.5, [S III] 18.6 and [Ar III] 9 μm. [b]IR5: IR4 + [N III] 57 μm. [c]IR7: IR5 + [O III] 88, [S IV] 10.5 μm. [d]IR11: IR7 + [Ne II] 12.8, [Ne III] 36, [S III] 33 and [Ar III] 21.8 μm.

9 μm). Out of these [N III] is peculiar since it has no optical counterpart and its predicted flux is again model-dependent. Accordingly, the most reliable, model-independent set is IR4, that is, IR5 minus [N III] 57 μm. A set including all IR CELs with reliable fluxes is IR7, that is, IR5 with the addition of [O III] 88 and [S IV] 10.5 μm. Finally, IR11 is the set including the 11 IR CELs that were well detected. In Table 4, the means and 1σ scatters in the departure ratios in models S1–S2 and D1–D2 are provided for the four line sets identified above.

The small scatter for IR4 indicates that an IR calibration from accurately measured lines can be reliably defined (with some reservations for D1), provided that these lines are weakly dependent on physical conditions. This suggests that the employed collisional/radiative atomic data and *ISO* observations are of fair accuracy, and that main features of the present models are not grossly in error. While our initial IR calibration is suited to models S1–S2, upward corrections of the IR line intensities by 19 and 39 per cent are indicated from D1 and D2, respectively. This shift is not a weakness of the D models since the absolute calibration of the

IR relative to the optical is rather poor: for example, note that the Hβ flux, as derived from the H I IR lines, is more than twice the one estimated by Dufour et al. (1982) falling into their *IUE* 10 × 20-arcsec² lobe [comparison made after reduction to an equally sized aperture; the SWS and Dufour et al. (1982) observed a very similar position]. Thus, an upward calibration of the IR lines relative to the optical serves to reduce the disagreement between these two $F(H\beta)$ estimates. In this respect model D2 should be preferred.

Upon adding [N III] (IR5), σ increases markedly for BB models (S1, D1), whereas it is stable for *CoStar* models (S2, D2), showing that, by adopting the latter primary spectrum, the consistency between the optical [N II] CELs (used to determine N/H abundance ratio) and the IR [N III] line is preserved. Considering IR7, which comprises all accurately measured IR CELs, σ is rather stable (and large) for S1 and D1, but is dramatically increased for S2 due to the large departure ratio of [S IV]. In contrast to S2, model D2 is only mildly affected, thanks to the conjunction of (i) a smaller departure ratio for [S IV] due to the relatively high pressure in the inner zone of this model, and (ii) an overall enhancement of the IR line intensities (the factor of 1.39 upward shift in calibration) partly due to the enhanced abundances of Si–Fe in the hydrogen-poor gas (see below).

The full IR11 set leads to a general decrease of the averages, with a correlatively larger σ, partly attributed to the lesser accuracy of the four additional lines. None the less, model D2 again fares better with a σ of ∼20 per cent, probably not much larger than the one expected a priori on the basis of the claimed accuracy of the employed line fluxes. The decrease of the averages from IR7 to IR11 is mainly due to [Ar III] 21.8 and [Ne II] 12.8 μm, with the former being by far the weakest line of the set and the latter strongly model-dependent, and hence relevant for model appraisal. The particularly bad score

of S1 and S2 when all IR CELs are included is to a large extent a consequence of the deficiency of the predicted [Ne II] intensity, while the acceptable score of D1 relates to an excellent fit to [Ne II]. Here the dual-abundance models constitute an improvement over the homogeneous models, with a large fraction of [Ne II] arising from the hydrogen-poor gas. In this respect, D2 may appear somewhat less successful than D1; the fact, however, that [Ne II] is underestimated in D2 does not necessarily imply a failure of the model, as the same occurs in an unpublished NEBU model of NGC 7027 using the same atomic data. Assuming on this basis a 50 per cent improvement to the [Ne II] 12.8-μm fit and ignoring [Ar III] 21.8 μm, the 1σ scatter in the departure ratios for the full set of IR CELs is only 14 per cent in D2.

Concerning elements beyond magnesium and owing to the large S/H and Ar/H abundance ratios in the hydrogen-poor component of model D2, the two most representative lines [S III] 18.7 and [Ar III] 9 μm are enhanced relative to D1, and are in harmony with the most representative IR CELs of nitrogen, oxygen and neon. This is the origin of the remarkably small scatter found for IR CELs in D2 (Fig. 2), indicating that elements beyond magnesium are potentially enhanced along with oxygen in the posited hydrogen-poor gas.

Another clue to the superiority of model D2 over D1 is provided by N II and [N II]. In model D1, the temperature of the hydrogen-poor gas is not low enough to fully quench the [N II] λ6584 emission, as O/H cannot be very large, given the constraint imposed by the weak O I λ7773 ORL. Since N/H there is bound to be sufficiently large to account for the N II λ5679 ORL, [N II] λ6584 is enhanced, which leads in turn to a decrease of N/H in the 'normal' component, with the consequence that [N II] λ5755, which was somewhat over-estimated in homogeneous models, is now underestimated (this line cannot be produced in the hydrogen-poor gas, because of its high excitation temperature). Lowering the overall N/H then leads to an increase of N/H in the hydrogen-poor gas in order to account for the N II ORL emission, thus potentially causing a kind of divergence of N/H abundance ratio in both the components, with an increasingly bad fit to the optical [N II] line ratio. Although this divergence does not really occur in D1, it can explain why the predicted [N II] λ5755/λ6584 ratio in D1 is significantly low (Table 3), and why the overall N/H abundance ratio in the same model is anomalously small (being almost equal to that in S1, contrary to all other abundances; see Table 2). On the other hand, the extra cooling provided by notably [S III] and [Ar III] in the hydrogen-poor component of D2 is enough to almost quench [N II] λ6584 emission, thus preventing the 'N II divergence' and leading to an optimal fit for the optical [N II] line ratio. In this sense, the dual-abundance models are generally more successful than their homogeneous counterparts and, among them, D2 is by far the most successful.

Finally, the scatter in the IR line departure ratios in D2 can be scrutinized from yet another standpoint. Among the four lines added to IR7 to make up IR11, the very strong [S III] 33 μm stands out. Adding this line only to IR7, σ increases from 12 to 15 per cent. As previously noted, [S III] 33 and [O III] 88 μm, are the only lines which can be seriously affected by collisional de-excitation in the low-density conditions of 30 Doradus. The average for the remaining six lines of IR7 is 1.42, close to the re-calibration factor of 1.39 obtained from IR4, and the scatter is again 8 per cent only (similar to that found for IR4 or IR5; Table 4). Thus after re-calibration, *all* strong IR CELs in D2 are predicted in remarkable agreement with observation, with the exception of [O III] 88 and [S III] 33 μm, which are both underestimated by a factor of ~1.3 (Fig. 2), suggesting that the fields of view of LWS and SWS-4 sampled regions of lower average density than the bright 'optical' filament. In a trial calculation with

R_{in} twice larger and the gas pressure one third that of model D2, the IR [O III] predicted line ratio was inverted, while the [S III] ratio was better fitted without being inverted; predictions for other IR CELs remained fair. This suggests that taking into account the background emission falling into the *ISO* lobe could help in improving the fit to [O III] 88 and [S III] 33 μm, although the [S III] line ratio would still be off somewhat. At this point we recall that the [S III] 33-μm line was not amongst the most accurately measured, and that the collision strengths for the [S III] IR CELs are probably not of ultimate accuracy; the values by Galavis et al. (1995) used in the present investigation, differ very substantially from those obtained by Tayal & Gupta (1999).

In conclusion, the few imperfections of model D2 can be naturally understood as a consequence of the coarseness of the 'one-filament approximation' and/or uncertainties in the observations and the atomic data. The global upward re-calibration of the IR line fluxes required by this model is warranted because the gap between the SWS and direct estimates for $F(H\beta)$ is then substantially narrowed. The dual-abundance models generally improve the fit to several lines other than the CNO ORLs, and D2 represents the most satisfactory compromise since the scatter in the departure ratios of IR CELs is much reduced. An important consequence of the above discussion is that it is quite plausible that the posited hydrogen-poor component is enriched (relative to H) not only in CNONe, but also in heavier elements.

3.4.3 Ionization structure

In Fig. 3, comparison is shown between the ionic fractions of N$^+$ and O$^+$ in the two gas phases of model D2, while in Figs 4 and 5 the comparison involves the ionic fractions of the doubly ionized species of CNONe in each of the two D2 nebular components. The IR [O III], [Ne III] and [S III] lines are the principal coolants in the clumped phase and are emitted instead of the optical [O III] coolants because they are favoured by the lower prevailing T_e, while the clump density ($N_e = 696\,cm^{-3}$) is not sufficient to severely quench most of the lines. In this respect, the model is in harmony with the suggestion made by T03 who, based on the observed deviations of O II ORL relative intensities from their theoretical LS-coupling ratios, proposed that the ORL emission in 30 Doradus (and other
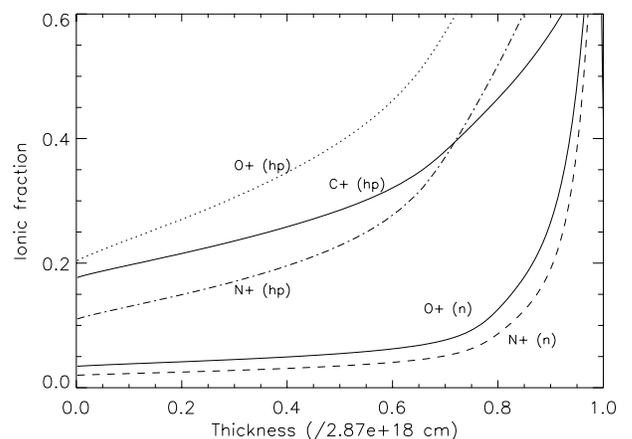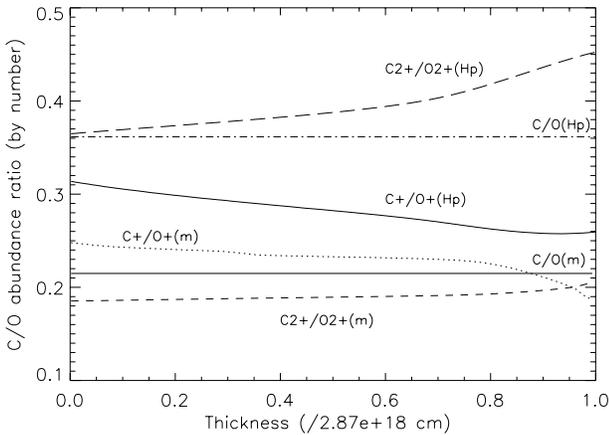

Figure 3. Ionic fractions of singly ionized carbon, nitrogen and oxygen in the hydrogen-poor and normal gas phases of model D2 versus the thickness of the model filament; 'n' and 'hp' labels as in Fig. 1.
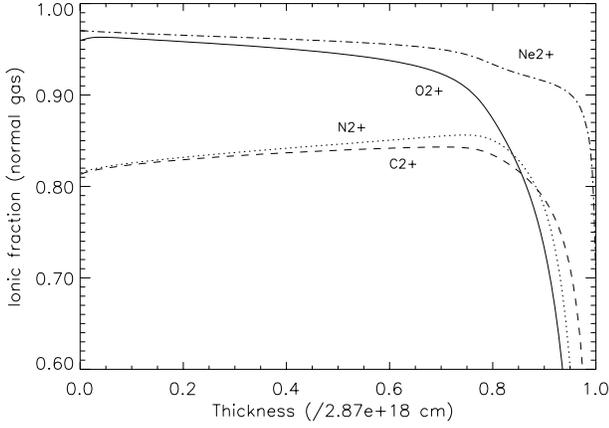
Figure 4. Ionic fractions of doubly ionized CNONe in the normal gas phase of model D2 versus thickness.
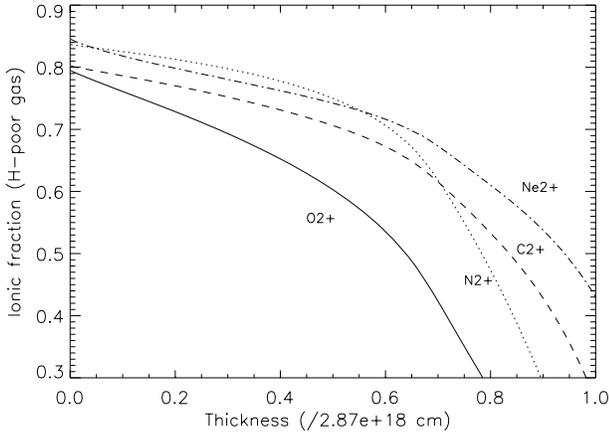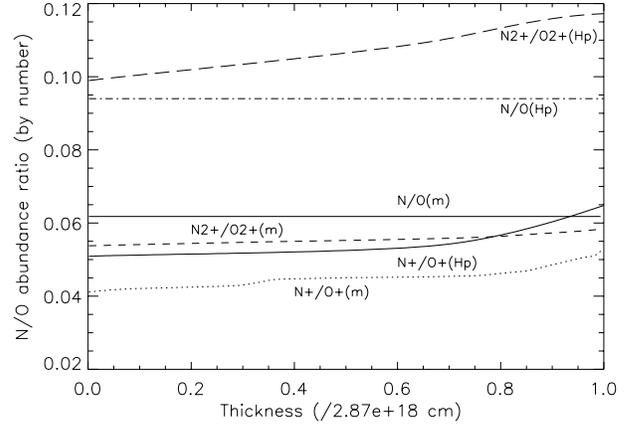

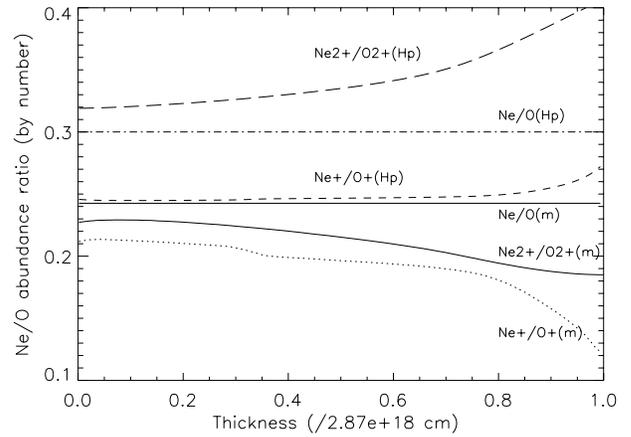**Figure 5.** As in Fig. 4, for the hydrogen-poor gas phase of model D2.

Figure 6. The C/O elemental and ionic abundance ratios in model D2 versus the thickness of model filament; curve labels marked by 'm' refer to mean quantities for the whole nebula, while those marked by 'hp' refer to quantities within the hydrogen-poor phase only.

Figure 7. As in Fig. 6, for N/O elemental and ionic abundance ratios.

Figure 8. As in Fig. 6, for Ne/O elemental and ionic abundance ratios.

HIIRs) originated in low-density regions and not in exceedingly dense, supposedly ionized clumps (see also Ruiz et al. 2003).

The variation of the ionic and elemental C/O, N/O and Ne/O abundance ratios across the nebula was studied (Figs 6–8). From a comparison with results obtained from observations, some in-

sight can be gained on the best way of determining these important quantities. Here, the model C/O, N/O and Ne/O abundance ratios (by number) are well approximated by the abundance ratio of their respective doubly ionized species, for example, $N/O \simeq N^{2+}/O^{2+}$ ($\neq N^{+}/O^{+}$). This is true for the *mean* abundance ratios for the whole nebula, as well as for the ratios within the relatively hydrogen-poor phase only, and is due to the high-excitation state of the gas. The N^{+}/O^{+} abundance ratio, often used as an approximation to the N/O abundance ratio by observers who sample the optical [N II] and [O II] CELs only, is about two third the mean elemental ratio, while in the clumps it is lower by a factor of 2 than the respective N/O abundance ratio of the hydrogen-poor phase. These results reproduce the behaviour of N/O obtained by T03 (cf. their table 12) based on pure optical and pure IR forbidden-line ratios. As was also noted by Rubin et al. (1988), Simpson et al. (1995) and T03, in several HIIRs IR fine structure (FS) line ratios yield a consistently higher N/O abundance ratio than optical-line ratios. According to the models shown here the IR FS lines of [N III] and [O III] give a better estimate of the N/O ratio than the optical [N II] and [O II] CELs, both for the nebula as a whole, and for the posited, embedded hydrogen-poor clumps also (if one was to image the clumps in IR nitrogen and oxygen fine-structure lines to derive their N/O abundance ratios). It should be mentioned that the same behaviour of the carbon, nitrogen and neon ratios relative to oxygen is obtained for the chemically homogeneous model S1.

3.5 On the t^2 factors from models

Modelled mean temperatures ($T_{0,i}$), mean-squared temperature-fluctuation (t^2) factors (Peimbert 1967) and ionic fractions (X^{+i}/X) are shown in Table 5 for the whole shell of model D2 (upper right-hand panel), the hydrogen-poor component (lower left-hand panel) and the normal component (lower right-hand panel) for the elements hydrogen, helium, carbon, nitrogen, oxygen, neon and sulphur; $T_{0,i}$ and t^2 values were derived using, for example, equations (3) and (4) of P03. Under the assumption for the existence of temperature fluctuations in a chemically homogeneous nebular medium, the elemental abundances derived from CELs overall underestimate the true abundances due to the adoption of a non-representative (over-estimated) electron temperature for all nebular zones. Under this premise the heavy-element ORLs, which in most cases yield higher

abundances than CELs, are often thought to give a more accurate measure of the nebular abundances since their strengths relative to Hβ are much less dependent on T_e (and N_e) than any given CEL to Hβ line ratio. Because of this, various workers have adopted a methodology whereby abundances of elements from carbon to iron, and derived from CELs, are often corrected upwards. The corrections are estimated by adopting a representative t^2 factor which is usually the average of those computed from the difference between the Balmer discontinuity and [O III] forbidden-line temperatures (t^2_{Bal}), and those computed from the ORL versus CEL ADF (t^2_{ADF}; for example, from C^{2+} and O^{2+} ions). P03 adopted $t^2 = 0.033$ for 30 Doradus corresponding to *rms* temperature fluctuations across the nebula of 18 per cent. Similar values were deduced from the O^{2+} ADFs by P03 and T03. Slightly higher values were found from the C^{2+} ADF by the same authors. Our

Table 5. Temperatures (in K), t^2 factors and mean neutral and ionic fractions, for the chemically homogeneous model S1, and the dual-abundance model D2 (for the whole nebula and each of the two components) for H, He, CNONe, and S. The numbers in parentheses are powers of 10.

Element		I	II	III	IV	I	II	III	IV
				S1				D2	
H	($T_{0,i}$)	9958	9962			10 920	9654		
	(t^2)	1.29 (−2)	4.45 (−3)			2.09 (−2)	2.23 (−2)		
	(X^{+i}/X)	9.66 (−3)	9.90 (−1)			8.03 (−3)	9.92 (−1)		
He		10 150	9960	9807		9741	9615	9174	
		1.28 (−2)	4.45 (−3)	1.65 (−5)		6.72 (−2)	2.52 (−2)	1.70 (−2)	
		9.35 (−3)	9.91 (−1)	1.57 (−4)		7.70 (−3)	9.92 (−1)	2.92 (−4)	
C		10 860	10 610	9904	9592	5421	6585	7821	9089
		3.76 (−3)	5.83 (−3)	3.92 (−3)	1.03 (−3)	2.11 (−1)	2.28 (−1)	1.44 (−1)	2.84 (−2)
		3.58 (−5)	9.92 (−2)	8.66 (−1)	3.45 (−2)	1.06 (−4)	1.99 (−1)	7.47 (−1)	5.31 (−2)
N		9433	10 790	9876	9600	7162	7129	7901	8789
		2.09 (−2)	4.68 (−3)	3.58 (−3)	1.12 (−3)	1.75 (−1)	2.07 (−1)	1.37 (−1)	5.17 (−2)
		2.49 (−3)	1.07 (−1)	8.53 (−1)	3.73 (−2)	1.60 (−3)	1.91 (−1)	7.40 (−1)	6.69 (−2)
O		9868	10 730	9818	9808	9570	7533	8679	8425
		1.33 (−2)	4.58 (−3)	3.06 (−3)	2.03 (−5)	9.45 (−2)	1.96 (−1)	7.78 (−2)	7.37 (−2)
		8.66 (−3)	1.58 (−1)	8.33 (−1)	6.48 (−5)	6.07 (−3)	2.30 (−1)	7.64 (−1)	7.10 (−5)
Ne		9172	10 380	9901	9797	5363	5843	8046	8031
		2.22 (−2)	5.58 (−3)	4.02 (−3)	2.45 (−5)	1.40 (−1)	2.27 (−1)	1.30 (−1)	1.04 (−1)
		1.33 (−3)	1.28 (−1)	8.71 (−1)	6.45 (−6)	8.13 (−4)	1.44 (−1)	8.56 (−1)	1.56 (−6)
S		10 270	10 550	10 130	9600	6885	8134	8348	9152
		1.03 (−2)	7.64 (−3)	4.90 (−3)	1.06 (−3)	2.38 (−1)	1.70 (−1)	1.20 (−1)	2.40 (−2)
		2.46 (−6)	3.31 (−2)	6.31 (−1)	3.21 (−1)	3.51 (−6)	5.49 (−2)	6.72 (−1)	2.52 (−1)
				D2 (hydrogen-poor gas)				D2 (normal gas)	
H	($T_{0,i}$)	5325	4120			10 500	9897		
	(t^2)	3.70 (−2)	6.29 (−2)			6.71 (−3)	7.20 (−3)		
	(X^{+i}/X)	3.04 (−2)	9.70 (−1)			1.80 (−2)	9.82 (−1)		
He		5158	4107	3128		10 370	9903	9407	
		4.48 (−2)	6.24 (−2)	1.51 (−4)		7.83 (−3)	7.23 (−3)	2.70 (−5)	
		4.79 (−2)	9.52 (−1)	2.05 (−4)		1.13 (−2)	9.88 (−1)	2.90 (−4)	
C		4699	4672	3847	3421	10 740	10 550	9850	9465
		5.42 (−2)	5.74 (−2)	5.17 (−2)	2.31 (−2)	6.63 (−3)	7.85 (−3)	6.68 (−3)	2.43 (−3)
		2.56 (−4)	3.80 (−1)	6.12 (−1)	7.89 (−3)	2.85 (−5)	1.26 (−1)	7.94 (−1)	7.95 (−2)
N		5304	4875	3718	3376	10 350	10 840	9800	9484
		3.62 (−2)	4.78 (−2)	4.10 (−2)	1.84 (−2)	8.26 (−3)	6.89 (−3)	5.96 (−3)	2.63 (−3)
		1.53 (−2)	3.64 (−1)	6.01 (−1)	1.97 (−2)	2.21 (−3)	1.30 (−1)	7.78 (−1)	9.04 (−2)
O		5510	4624	3601	3131	10 460	10 790	9736	9407
		2.67 (−2)	5.38 (−2)	3.45 (−2)	1.48 (−4)	6.45 (−3)	7.38 (−3)	5.35 (−3)	5.11 (−5)
		2.81 (−2)	4.91 (−1)	4.81 (−1)	4.07 (−5)	1.59 (−2)	1.52 (−1)	8.32 (−1)	7.85 (−5)
Ne		5175	4587	3946	3129	9864	10 250	9885	9393
		4.61 (−2)	5.93 (−2)	5.81 (−2)	2.88(−4)	7.00 (−3)	8.11 (−3)	7.11 (−3)	3.95 (−5)
		6.43 (−3)	3.17 (−1)	6.77 (−1)	8.48 (−7)	6.15 (−4)	6.26 (−2)	9.37 (−1)	1.91 (−6)
S		4839	4933	4070	3378	10 590	10 740	10 080	9465
		5.55 (−2)	5.24 (−2)	5.95 (−2)	1.96 (−2)	6.61 (−3)	6.64 (−3)	7.71 (−3)	2.32 (−3)
		1.23 (−5)	1.43 (−1)	8.05 (−1)	5.22 (−2)	3.00 (−6)	5.22 (−2)	6.16 (−1)	3.05 (−1)

Table 6. Gas-phase abundances (by number) from single- and dual-abundance models compared to empirical abundances, in units such that $\log N(\text{H}) = 12$.

	S1	S2	D1 Mean	D2 Mean	This work adopted	P03[a] $t^2 = 0.0$	P03[a] $t^2 = 0.033$	T03[b] $t^2 = 0.0$	V02[c] $t^2 = 0.0$
He	10.93	10.93	10.92	10.92	10.92	10.94	10.93	10.96	10.97
C	7.64	7.66	7.78	7.78	7.78	7.80	8.05	–	–
N	7.24	7.15	7.25	7.24	7.24	7.05	7.21	6.89	6.84
O	8.36	8.37	8.45	8.45	8.45	8.33	8.54	8.34	8.25
Ne	7.64	7.60	7.73	7.73	7.73	7.65	7.83	7.66	7.84
Mg	6.72	6.60	6.74	6.65	6.69	–	–	–	–
Si	6.40	6.45	6.46	6.53	6.50	–	–	–	–
S	6.79	6.83	6.83	6.85	6.84	6.84	6.99	6.77	6.82
C	4.77	4.84	4.82	4.90	4.87	4.75	4.82	4.85	–
Ar	6.08	6.10	6.12	6.16	6.14	6.09	6.26	6.15	6.21
Fe	6.07	6.04	6.14	6.11	6.12	6.25	6.39	–	–

[a]Peimbert (2003). [b]Tsamis et al. (2003a). [c]Vermeij & van der Hulst J. M. (2002).

modelling results, however, allow for an alternative interpretation of the observations.

The single-component, chemically homogeneous model S1 yields $t^2(\text{H}^+) = 0.0045$, that is, the *rms* T_e fluctuations over the whole H II zone are 7 per cent (Table 5). Previous work on photoionization nebular models under the assumption of chemical homogeneity and variable gas density did not reveal t^2 factors much in excess of ~ 0.01 for a wide range of ionizing colour temperatures and densities (Kingdon & Ferland 1995, hereafter KF95). In model S1 the t^2 factors for doubly ionized CNONe are all less than $t^2(\text{H}^+)$ as they should be; this is a well-known result (Harrington et al. 1982; KF95) arising from the non-coincidence of the H$^+$ and O^{2+} zones. KF95 warn against a direct comparison between t^2_{Bal} and model-derived t^2 factors, such as those listed in Table 5, because the comparison is valid only when the mean ionic temperatures and t^2 factors for H$^+$ and O^{2+} are equal. This is not exactly true even for our chemically homogeneous model S1 where $T_{0,i}(\text{O}^{2+}) - T_{0,i}(\text{H}^+) = -144$ K and $t^2(\text{O}^{2+}) = 0.69 t^2(\text{H}^+)$. For the dual-abundance model D1, these values are -975 K and $3.5 t^2(\text{H}^+)$, respectively. P03 found $t^2_{\text{Bal}} = 0.022$, interpreting this result as evidence for temperature fluctuations in a chemically homogeneous nebula. This is not supported by model S1. It should further be noted that both S1 and D1 models fit the Balmer discontinuity within a 3 per cent margin (as well as the optical [O III] lines). Only models D1–D2, however, reproduce the intensities of the CNO ORLs. For model D2 globally, $t^2(\text{H}^+) = 0.022$, $t^2(\text{O}^{2+}) = 0.078$ and $t^2(\text{C}^{2+}) = 0.14$; thus the introduction of hydrogen-deficient inclusions results in the derivation of higher t^2 values that approach or exceed the (empirical) t^2_{Bal}. Even so, this verisimilitude cannot be interpreted in the framework of the original T_e-fluctuation hypothesis since the empirical t^2_{Bal} has no direct physical correspondence in the context of these models. This is also evident from Fig. 1 where the electron-temperature profile across the physical extent of the two gas phases of model D2 is plotted. A substantial temperature gradient can only be discerned throughout the hydrogen-poor phase whose T_e rises, almost monotonically, from ~ 3000 K at the inner edge to 6200 K at the outer model radius. Similarly, the empirical t^2_{ADF} values cannot be meaningfully compared with the t^2 values of the model for various ions.

3.6 Model *versus* empirical t^2 elemental abundances

The abundances derived from our four models are presented in Table 6 (columns 2–5), along with our adopted preferred estimates

(column 6; mean of models D1 and D2) and those from previous determinations (columns 7–10). They do not include estimates for depletion onto dust grains, so they pertain to the gaseous phase only. Both the $t^2 = 0.0$ and 0.033 results of P03 are listed (the latter were favoured by P03). Our preferred abundances are lower overall than those for $t^2 = 0.033$, but nitrogen is 10 per cent larger; this is partly due to the coarse correction for unseen ions applied by P03 (see Section 3.4.3). The differences are largest, about a factor of 2, for carbon and iron. These are the elements which are mostly affected by the upward correction under the assumption of $t^2 = 0.033$.

At this point it should be noted that abundances determined from detailed photoionization models and empirical methods cannot be immediately ranked. Models have the obvious advantage of self-consistency and of optimized (although possibly wrong) ionization correction factors, whereas empirical methods exactly 'fit' diagnostic lines by definition. The presented models exactly fit all the standard diagnostic lines. While this accuracy is illusory for obvious reasons, it does ensure that, for given atomic data, the model abundances arguably supersede the empirical ones.

The $t^2 \neq 0$ empirical approach not only supersedes the classical one ($t^2 = 0$) in that it integrates new spectral features, but also it takes advantage of fitting approximately the heavy-element ORLs to claim superiority over models which do not fit them, despite the fact that there is no strong physical basis for the existence of large-amplitude temperature fluctuations in chemically homogeneous nebulae.[5] Here we exhibit photoionization models based on known standard physics, which account for the ORLs as well as for other optical spectroscopic diagnostics, thanks to the fundamental assumption of chemical inhomogeneity, which we consider to be plausible on independent grounds (Section 4). In addition, despite the demanding condition of physical self-consistency, the models account well for a number of independent observables, while the remaining moderate discrepancies are understood in terms of identified uncertainties and the coarseness of the single-filament description. Therefore, even though the models are probably not unique, their (averaged) abundances provide a basis on which empirical t^2 abundances can be evaluated in this particular situation.

A comparison of the results is meaningful if differences in the employed atomic data and possible inaccuracies in the

[5] It should be noted, however, that Stasińska & Szczerba (2001) proposed nebular models which resulted in enhanced t^2 values by considering small-scale density variations in a dusty medium.

© 2005 The Authors. Journal compilation © 2005 RAS, MNRAS **364**, 687–704

ionization correction factors adopted in the empirical approach are neutralized. This can be achieved by considering the results *differentially*. For this purpose, the $t^2 = 0$ abundances obtained by P03 can be associated to models S1–S2 (fit to optical/UV CELs), and the $t^2 = 0.033$ abundances to models D1–D2 (fit to both optical/UV CELs and ORLs). Excluding helium and elements not considered by P03, the average abundance ratios of D1 over S1 and D2 over S2 are both equal to 1.20 ± 0.10 (the aberrant nitrogen abundance of D1 was discarded; see discussion on [N II] in Section 3.4.2), while the same ratio for the '$t^2 = 0.033$' over '$t^2 = 0$' abundances is 1.48 ± 0.18. Although we have no clear explanation of why this is so, we note that the *square root* of the 't^2 abundance ratio', 1.21 ± 0.07, is identical to the 'D/S model ratio' (on close inspection of Table 6, however, the individual abundance enhancements differ significantly in the two approaches). Thus, compared to this particular self-consistent physical model which quantitatively accounts for observation, the '$t^2 = 0.033$' abundances are significant overestimates, while the mean D1–D2 model abundances are equal on average to the geometric mean of the $t^2 = 0$ and non-zero empirical abundances. In other words, *there is objectively no reason in this example to prefer one or the other set of empirical abundances*. On the other hand, concerning physical models, it is noted that whereas a model which fits existing observational data might be wrong, one which does not almost certainly is. On these grounds we deem that adopting average abundances from models D1–D2 as representatives is a justified improvement compared to values derived from either chemically homogeneous models or empirical methods.

3.7 On the composition of the hydrogen-poor gas

3.7.1 Helium and the primordial helium abundance

The question of whether helium is enriched in the clumped gas along with CNONe is of interest, since helium is expected to be present in, for example, nucleosynthetic products expelled from evolved, massive WR-type stars (e.g. Rosa & Mathis 1987; Kobulnicky et al. 1997). The larger the helium abundance is in the hydrogen-deficient gas, the smaller it is in the 'normal' nebular component. A recent value for the primordial He/H is about 0.0786 by number (Luridiana, Peimbert & Peimbert 2003). From model trials, the condition that He/H > 0.08 in the normal component translates into He/H < 0.12 for the posited hydrogen-poor clumps in 30 Doradus. Thus, helium is not much enhanced relative to hydrogen in the clumps, and the excess heavier elements there should originate in extreme nucleosynthesis of the kind expected from supernova (SN) explosions (e.g. Woosley, Heger & Weaver 2002), rather than from Wolf–Rayet stellar winds (see Section 4).

In both D1 and D2, He/H = 0.10, was arbitrarily adopted for the hydrogen-poor component (between the extremes of 0.08 and 0.12; Table 2). Decreasing He/H in the clumps below 0.10, an increase of the *overall* He/H abundance ratio follows until the latter becomes approximately equal to the one found from chemically homogeneous models (or standard empirical analyses). If, reasonably, it is assumed that He/H in the hydrogen-poor gas is at least as large as in the normal gas, it naturally follows that the He/H abundance ratio derived from standard analyses of HIIRs, under the assumption of nebular chemical homogeneity, is only an *upper limit to the actual helium abundance*. A similar point was made by Péquignot et al. (2002) in the case of PNe. This systematic effect is a possible new source of uncertainty in the important quest for the primordial helium abundance from GHIIR spectroscopy of blue compact galaxies (e.g. Luridiana et al. 2003; Izotov & Thuan 2004).

3.7.2 Elements beyond helium

While the major part of oxygen and other heavy elements, such as neon, magnesium, silicon, sulphur, chlorine and argon, is ejected into the ISM during the final stages of massive star evolution ($M > 8\,M_\odot$) and the resulting Type II SN explosions, the exact contribution of massive stars versus low- and intermediate-mass stars in the production of carbon and nitrogen is under debate: for example, Carigi et al. (2005) advocate Galactic chemical evolution models according to which only about half of the carbon found at present in the solar vicinity has been produced by massive stars. SN ejecta are strongly deficient in hydrogen and constitute promising sources of 'oxygen-rich clumps' such as those favoured in the present work (see also Section 4). Are then the CNO(Ne) abundances of the hydrogen-deficient clumps discussed herein in keeping with those expected from massive star nucleosynthesis? First, it must be noted that the photoionization model abundances for such hydrogen-poor clumps are likely to be affected by large uncertainties. Concerning nitrogen in particular, only a few weak N II ORLs are available, which can result in an overestimated N/O abundance ratio in cases of unforseen blends with even weaker lines; in addition, the N II lines belonging to multiplet V3 are known to be potentially partly excited by continuum fluorescence, not only by recombination (see e.g. T03); this also points towards an upper limit N/O abundance ratio for the hydrogen-poor gas. The weakness of the N II ORLs certainly implies that the N/O abundance ratio of the posited clumps is much less than unity, but it does not provide a precise value or even a secure lower limit. More generally, uncertainties can also arise from the fact that the abundances of the clumps were obtained from recombination lines *after* subtracting the contribution to their emission from the 'normal' composition nebular gas (40–50, 50–70 and 65–70 per cent for C II, N II and O II ORLs, respectively). Thus, while there is absolutely no doubt that the observed intensities of at least the C II and O II ORLs are larger than those obtained from chemically homogeneous models,[6] the exact excess, here some 55, 40 and 30 per cent for C II, N II and O II, respectively, is not very accurately determined due to observational uncertainties. Another source of uncertainty in the resulting abundances is the coarseness of the sampling of the material effectively observed, given the necessarily schematic geometry of the dual-abundance photoionization model and the fact that spatially resolved observations of the posited hydrogen-poor clumps are not available yet; the latter goal might some day be achieved via means of integral-field unit spectroscopy with very large telescopes.

If we consider that our model hydrogen-poor clumps would in reality correspond to a homogeneous mixture of extremely hydrogen-deficient material to which 'normal' ISM gas has been partially introduced, the (corrected) relative abundances in the model clumps of (C/O, N/O) ∼(0.36, 0.09) (model D2; Table 2) can be compared to the (C/O, N/O) ∼(0.20, 0.03) abundance ratios expected from typical massive star nucleosynthesis for the pre-SN wind *plus* Type II SN ejecta (cf. fig. 27 of Woosley et al. 2002). The fact that the photoionization models tend to indicate C/O and N/O abundance ratios 2–3 times larger than 'expected' may be a potential difficulty for either the model assumptions or the proposed origin of the posited

---

[6] As mentioned in Section 1 this is amply documented in empirical analyses of many HIIRs (Peimbert et al. 1993; Esteban et al. 2005), including 30 Doradus (T03; P03).

clumps, and requires further analysis: the details of the mixing process of hydrogen-poor with hydrogen-rich gas should especially be investigated. The same conclusion applies to Ne/O, although in this case only upper limits to the Ne II ORLs are available and Ne/O relies on IR CELs, notably the [Ne II] 12.8-μm transition (25–30 per cent flux accuracy). None the less, keeping in mind the aforementioned uncertainties, the departures between model results and massive star nucleosynthetic theory are not large enough to jeopardize the basic features of the model. The N/O abundance ratio is found to be definitely very small in the hydrogen-poor gas and therefore satisfactory at the semi-quantitative level currently attainable, even for cases where part of the nitrogen that was ejected during the pre-SN evolution might not reside in oxygen-rich clumps. On the other hand, the determination of C/O abundance ratio in the ISM of the LMC involves the difficult calibration of the C III] λ1909 intensity relative to the optical, which in turn can impact the accuracy of the estimated contribution of the 'normal' gas to the emission of C II λ4267. Finally, the photoionization model analysis indicates that the IR lines are overall best accounted for by model D2 in which elements heavier than neon, such as the essentially better-constrained sulphur and argon, are enhanced in the hydrogen-poor gas by similar amounts to oxygen (Section 3.4.2); this is expected for material akin to Type II SN ejecta.

4 DISCUSSION AND CONCLUSIONS

Self-consistent photoionization models of the giant 30 Doradus nebula in the LMC have been constructed, precisely fitting all the optical spectroscopic plasma diagnostics available for a bright filament observed from UV to radio wavelengths. A dual-abundance model (D2) is favoured which incorporates small-scale chemical inhomogeneities in the form of relatively hydrogen-deficient inclusions embedded in gas of typical LMC composition, and subjected to a *CoStar* model-atmosphere ionizing spectrum. The model filament, whose gas pressure increases outwards by a factor of 2, is essentially radiation bounded and its geometrical thickness and distance from the central source are in good agreement with what is suggested from Hβ images of the nebula. The relatively cool and dense inclusions are uniformly distributed throughout the filament and are in local pressure equilibrium with their surroundings, representing 2 per cent of the nebular mass, while emitting about 8 per cent of the total Hβ flux. This model, designed to closely fit the CNO ORLs (in addition to the UV/optical CELs), leads to significantly improved predicted intensities for a number of other optical and IR lines, which were not used in the convergence process. The helium abundance relative to hydrogen is about normal in the inclusions, while all other elements for which enough information is available (carbon, nitrogen, oxygen, neon, sulphur and argon) have abundances that are enhanced by typically one order of magnitude compared to their respective values in the ambient HIIR. To our knowledge, this is the first time that an HIIR model is exhibited which, incorporating only standard, dust-free physics for photoionized nebulae, provides a satisfactory solution to the extensively researched issue of discordant ORL versus CEL heavy-element abundances in this class of objects.

The abundances of heavy elements in the chemically inhomogeneous 30 Doradus models were found to be lower than those advocated by authors who consistently apply upward corrections to the forbidden-line abundances of HIIRs by postulating temperature fluctuations in a chemically homogeneous medium. For this particular nebula, the presence of hydrogen-deficient inclusions warrants an overall upward revision of the heavy-element abundances

by at most 0.1 dex, compared to empirical methods or models that do not take into account the heavy-element ORLs, and indicates that the latter techniques provide only an upper limit to the helium abundance in HIIRs. In as much as, in the current paradigm, the recombination lines do not provide an accurate estimate of the *overall* heavy-element to hydrogen-abundance ratios in a nebula, our findings cast new light on the use of CNONe ORLs as tracers of abundance gradients across galactic discs such as those exhibited by Esteban et al. (2005). It could prove worthwhile to investigate these gradients further in the context of dual-abundance HIIR models.

Notwithstanding the positive aspects of the presented models, we must ask ourselves: is there any basis to justify the existence of hydrogen-deficient inclusions in 30 Doradus or other HIIRs and what could their origins be? It is often argued that since the ISM appears to be chemically homogeneous (e.g. Moos et al. 2002; André et al. 2003), extensive mixing of the various chemical species should somehow occur. However, observations establish homogeneity by comparing different sightlines over typical ISM depths of ∼1 kpc, many orders of magnitude larger than the inclusions considered here. In fact, the 0.5-kpc local bubble appears to be oxygen deficient relative to the average few kpc neighbourhood (André et al. 2003). Our interpretation of 30 Doradus as a nebula which appears to be homogeneous on a large scale, but is chemically *inhomogeneous* at the smallest subparsec-sized scale, resonates with the findings of de Avillez & Mac Low (2002) who studied the mixing of chemical species in the ISM in the context of SN-driven models and concluded that: 'even if the major fraction of the ISM gas is completely mixed, lower level inhomogeneities will still be seen as abundances are measured more carefully'. We take it that the recent wealth of abundance determinations in nebulae involving ORLs, and extensively quoted in this work, has indeed increased the level of accuracy with which such studies can be done. Those authors established that the *smallest* ISM mixing time-scale, corresponding to the largest assumed SN explosion rate, is about 120 Myr, with weak abundance inhomogeneities taking longer times to be erased than strong ones due to an exponentially declining mixing rate for weaker inhomogeneities. As they noted, however, this representative time-scale is longer than the time interval between Type II SNe and other polluting factors, such as, for example, hydrogen-deficient winds from evolved massive stars or star formation debris, which in the meantime introduce fresh inhomogeneities into the ISM; it is also longer than the typical lifetime of HIIRs like 30 Doradus and their embedded stellar OB associations. Therefore, according to the study of de Avillez & Mac Low (2002), the ISM may never reach homogeneity under such conditions.

In an attractive scenario, Tenorio-Tagle (1996, hereafter TT96) proposes that, after a long journey in a hot coronal phase ($T \geqslant 10^6$ K), metal-rich material ejected by SNe erupting within OB associations will eventually fall back on to the galactic disc as a rain of cool, dense 'droplets' of final typical size of ∼10^{17} cm and densities of ∼10^3 cm^{-3}. These will be incorporated quite evenly into the atomic hydrogen and molecular hydrogen content of the disc, without significant mixing, until a next generation of massive stars photoionizes the gas and triggers complete mixing. Thus according to TT96, chemical homogeneity in a galactic disc is not instantaneously achieved soon after the end of a starburst event, but results as a consequence of the birth of the next massive star generation. It is tempting to identify the remains of the droplets singled out by TT96 with the hydrogen-deficient clumps introduced in the present photoionization models, especially as their size, a few percent of the size of a complete photoionized filament, and expected densities, ideally fits our needs. According to this depiction, one can

envisage a galaxy's ISM abounding with small-scale chemical inhomogeneities which are only observed emitting metallic recombination lines, such as C II λ4267, upon their photoionization in the vicinity of a young stellar cluster. In this context, we note that whereas the R136 cluster within 30 Doradus is of young age (1–5 Myr; Massey & Hunter 1998) and only few SNRs have been unambiguously identified in its wider vicinity (Lazendic et al. 2003; Chu et al. 2004), the older association Hodge 301 located 3 arcmin to the north-west, may have hosted ∼40 SNe since its formation 20–25 Myr ago according to estimates by Grebel & Chu (2000).

As emphasized by Scalo & Elmegreen (2004), a general problem with time-scale arguments pertaining to ISM mixing, is that they apply to turbulent transport (e.g. Roy & Kunth 1995), and *not* to chemical homogenization. For genuine mixing to be effectively achieved, viscosity and molecular diffusion are ultimately required, but these mechanisms act over very small scalelengths and/or very long times. Molecular diffusion becomes effective in the presence of strong gradients of concentration, for example, at the interface of two media with very different compositions. None the less, the *different thermal behaviours* of such media could also delay the mixing. This is a very complex problem for which a generic solution has yet to be found. Along the same lines, the detailed simulations of de Avillez & Mac Low (2002) point to a very long time-scale, over 10^8 yr, for the final decay of small ISM inhomogeneities. Future work may involve a coupled hydrodynamics–photoionization computational approach to this problem (e.g. Lim & Mellema 2003).

In the last step of the scenario developed by TT96, the disruption of the hydrogen-poor droplets by photoionization proceeds hydrodynamically aided by the presence of shocks, and the gas, now at 10^4 K, acquires densities similar to those of the ambient HIIR; diffusion of the disrupted droplets is then suddenly accelerated. TT96 estimated a final diffusion time of the order of 10^4 yr in the lowest density HIIR gas (at the small spatial scale of the metal-rich droplets), and a time significantly shorter than 10^6 yr in denser filaments. At first view, this time-scale for complete chemical homogenization in the newly born HIIR seems uncomfortably short to justify identification of the droplets with the hydrogen-poor clumps posited in the present photoionization models. Importantly however, we note that, unlike the supposition made by TT96, even in the event of its re-ionization, the hydrogen-poor gas can *maintain* a very low temperature due to fine-structure line cooling and *remain* relatively dense and isolated from its surroundings for some time. Thus, considering that the thermal properties of the hydrogen-poor inclusions will tend to significantly delay diffusion, it is quite possible that chemical inhomogeneities will survive for a significant fraction of the lifetime of a GHIIR. Under these conditions, identification of our model hydrogen-deficient clumps with the relics of the metal-rich droplets of T96 appears to be a reasonable guess. Additional work will be needed to develop observational tests of the model and to further constrain the abundances in the oxygen-rich inclusions. Whether a significant amount of nitrogen is present or not in the hydrogen-poor phase is critical with regard to the latter's origin in material lost, for example, during the pre-SN evolution of massive stars or in a Type II SN event (Section 3.7.2). Confirming with improved accuracy that elements beyond neon are overabundant in the clumps in the same way as oxygen (Section 3.4.2), is equally important.

In conclusion, the photoionization model description proposed here, which primarily aimed at quantitatively solving a longstanding spectroscopic anomaly using known, conventional HIIR physics, also turns out to be in qualitative agreement with independent theoretical considerations regarding the chemical evolution of the ISM. Detailed studies of other young, relatively metal-poor GHIIRs, such as 30 Doradus, may be a promising way to unravel small-scale composition inhomogeneities and provide additional observational support to the interesting thesis advocated by TT96. Efforts should be made for the detection of ORLs such as C II λ4267 and O II λ4650 (and others of nitrogen and neon ions) in HIIRs of all kinds, in order to build abundance determinations on firm grounds. Whether chemical inhomogeneity will prove to be the rule or the exception is an important question in its own right.

We note that the survival of hydrogen-deficient inclusions in the ISM could be of paramount importance for the process of star formation since these inclusions, cooler and denser than their surroundings, could act as seeds to trigger protostellar collapse.

REFERENCES

Allende Prieto C., Lambert D. L., 2001, ApJ, 556, L63
André M. K., Oliveira C. M., Howk J. C. et al., 2003, ApJ, 591, 1000
Barker T., 1984, ApJ, 284, 589
Berrington K. A., Burke P. G., 1981, Planet Space Sci, 29, 377
Blum R. D., Pradhan A. K., 1992, ApJS, 80, 425
Carigi L., Peimbert M., Esteban C., García-Rojas J., 2005, ApJ, 623, 213
Chu Y.-H., Kennicutt R. C., 1994, Astrophys Space Sci, 216, 253
Chu Y., Gruendl R. A., Chen C.-H. R., Lazendic J. S., Dickel J. R., 2004, ApJ, 615, 727
Crowther P. A., Dessart L., 1998, MNRAS, 296, 622
de Avillez M. A., Mac Low M., 2002, ApJ, 581, 1047
Dopita M. A., Sutherland R. S., 2000, ApJ, 539, 742
Dufour R. J., Shields G. A., Talbot R. J. Jr, 1982, ApJ, 252, 461
Ercolano B., Barlow M. J., Storey P. J., Liu X.-W., Rauch T., Werner K., 2003, MNRAS, 344, 1145
Esteban C., Peimbert M., Torres-Peimbert S., Rodríguez M., 2002, ApJ, 581, 241
Esteban C., García-Rojas J., Peimbert M., Peimbert A., Ruiz M. T., Rodríguez M., Carigi L., 2005, ApJ, 618, L95
Exter K. M., Barlow M. J., Walton N. A., 2004, MNRAS, 349, 1291
Filipovic M. D., Haynes R. F., White G. L., Jones P. A., Klein U., Wielebinski R., 1995, A&AS, 111, 311
Galavis M. E., Mendoza C., Zeippen C. J., 1995, A&AS, 111, 347
Galavis M. E., Mendoza C., Zeippen C. J., 1998, A&AS, 133, 245
Garnett D. R., Skillman E. D., Dufour R. J., Peimbert M., Torres-Peimbert S., Terlevich R., Terlevich E., Shields G. A., 1995a, ApJ, 443, 64
Garnett D. R., Dufour R. J., Peimbert M., Torres-Peimbert S., Shields G. A., Skillman E. D., Terlevich E., Terlevich R. J., 1995b, ApJ, 449, L77
Giveon U., Sternberg A., Lutz D., Feuchtgruber H., Pauldrach A. W. A., 2002, ApJ, 566, 880
Grebel E. K., Chu Y., 2000, AJ, 119, 787
Harrington J. P., Seaton M. J., Adams S., Lutz J. H., 1982, MNRAS, 199, 517
Hudson C. E., Bell K. L., 2005, A&A, 430, 725
Ibsen et al., 1983, ApJ, 264, 605
Israel F. P., Koornneef J., 1979, ApJ, 230, 390
Izotov Y. I., Thuan T. X., 2004, ApJ, 602, 200
Kennicutt R. C., Hodge P. W., 1986, ApJ, 306, 130
Kingsburgh R. L., Barlow M. J., 1994, MNRAS, 271, 257
Kingdon J., Ferland G. J., 1995, ApJ, 450, 691 (KF95)
Kobulnicky H. A., Skillman E. D., Roy J., Walsh J. R., Rosa M. R., 1997, ApJ, 477, 679

Lazendic J. S., Dickel J. R., Jones P. A., 2003, ApJ, 596, 287

Lim A. J., Mellema G., 2003, A&A, 405, 189

Liu X.-W., Storey P. J., Barlow M. J., Clegg R. E. S., 1995, MNRAS, 272, 369

Liu X.-W., Storey P. J., Barlow M. J., Danziger I. J., Cohen M., Bryce M., 2000, MNRAS, 312, 585

Liu X.-W., Luo S.-G., Barlow M. J., Danziger I. J., Storey P. J., 2001, MNRAS, 327, 141

Liu Y., Liu X.-W., Barlow M. J., Luo S.-G., 2004, MNRAS, 353, 1251

Luridiana V., Peimbert A., Peimbert M., Cerviño M., 2003, ApJ, 592, 846

Martins F., Schaerer D., Hillier D. J., 2002, A&A, 382, 999

Martín-Hernández N. L., Vermeij R., Tielens A. G. G. M., van der Hulst J. M., Peeters E., 2002, A&A, 389, 286

Mendoza C., 1983, Proc. IAU Symp. 103, Planetary Nebulae. Kluwer, Dordrecht, 143

Massey P., Hunter D. A., 1998, ApJ, 493, 180

Rosa M., Mathis J. S., 1987, ApJ, 317, 163

Mills B. Y., Turtle A. J., Watkinson A., 1978, MNRAS, 185, 263

Moos H. W., Sembach K. R., Vidal-Madjar A. et al., 2002, ApJS, 140, 3

O'Dell C. R., Peimbert M., Peimbert A., 2003, AJ, 125, 2590

Osterbrock D., 1989, Astrophysics of Gaseous Nebulae and Active Galactic Nuclei. University Science Books, Mill Valley, CA

Parker J. W., 1993, AJ, 106, 560

Peimbert M., 1967, ApJ, 150, 825

Peimbert A., 2003, ApJ, 584, 735 (P03)

Peimbert M., Peimbert A., Ruiz M. T., Esteban C., 2004, ApJS, 150, 431

Peimbert M., Storey P. J., Torres-Peimbert S., 1993, ApJ, 414, 626

Péquignot D., Amara M., Liu X.-W., Barlow M. J., Storey P. J., Morisset C., Torres-Peimbert S., Peimbert M., 2002, RMxAA (Ser. de Conf.), 12, 142

Péquignot D. et al., 2001, in Ferland G., Savin D. W., eds, ASP Conf. Ser. Vol. 247, Spectroscopic Challenges of Photoionized Plasmas. Astron. Soc. Pac., San Francisco, p. 533

Péquignot D., Liu X.-W., Barlow M. J., Storey P. J., Morisset C., 2003, in Kwok S., Dopita M., Sutherland R., eds, Proc. IAU Symp. 209, Planetary Nebulae: Their Evolution and Role in the Universe. Astron. Soc. Pac., San Francisco, p. 347

Rola C., Stasińska G., 1994, A&A, 281, 199

Roy J.-R., Kunth D., 1995, A&A, 294, 432

Rubin R. H., 1989, ApJS, 69, 897

Rubin R. H., Simpson J. P., Erickson E. F., Haas M. R., 1988, ApJ, 327, 377

Rubin R. H., Martin P. G., Dufour R. J., Ferland G. J., Blagrave K. P. M., Liu X.-W., Nguyen J. F., Baldwin J. A., 2003, MNRAS, 340, 362

Ruiz M. T., Peimbert A., Peimbert M., Esteban C., 2003, ApJ, 595, 247

Scalo J., Elmegreen B. G., 2004, ARA&A, 42, 275

Schaerer D., de Koter A., 1997, A&A, 322, 598

Simpson J. P., Colgan S. W. J., Rubin R. H., Erickson E. F., Haas M. R., 1995, ApJ, 444, 721

Stafford R. P., Bell K. L., Hibbert A., 1994, MNRAS, 266, 715

Stasińska G., Szczerba R., 2001, A&A, 379, 1024

Storey P. J., Hummer D. G., 1995, MNRAS, 272, 41

Tayal S. S., 2000, Atomic Data and Nuclear Data Tables, 76, 191

Tayal S. S., Gupta G. P., 1999, ApJ, 526, 544

Tenorio-Tagle G., 1996, AJ, 111, 1641 (TT96)

Tsamis Y. G., 2002, PhD thesis, University of London

Tsamis Y. G., Barlow M. J., Liu X.-W., Danziger I. J., Storey P. J., 2003a, MNRAS, 338, 687 (T03)

Tsamis Y. G., Barlow M. J., Liu X.-W., Danziger I. J., Storey P. J., 2003b, MNRAS, 345, 186

Tsamis Y. G., Barlow M. J., Liu X.-W., Storey P. J., Danziger I. J., 2004, MNRAS, 353, 953

Tsamis Y. G., Péquignot D., 2004, in Proc. ESO Workshop, Planetary Nebulae beyond the Milky Way. Springer-Verlag, Berlin, in press (astro-ph/0407506)

Tylenda R., 2003, in Kwok S., Dopita M., Sutherland R., eds, Proc. IAU Symp. 209, Planetary Nebulae: Their Evolution and Role in the Universe. Astron. Soc. Pac., San Francisco, p. 389

Vacca W. D., Garmany C. D., Shull J. M., 1996, ApJ, 460, 914

Vermeij R., van der Hulst J. M., 2002, A&A, 391, 1081

Vermeij R., Damour F., van der Hulst J. M., Baluteau J.-P., 2002, A&A, 390, 649

Wesson R., Liu X.-W., Barlow M. J., 2003, MNRAS, 340, 253

Woosley S. E., Heger A., Weaver T. A., 2002, Rev Mod Phys, 74, 1015

This paper has been typeset from a TeX/LaTeX file prepared by the author.